

Peripherally octamethyl zinc(II) phthalocyanines with various axial substituents

Jan Janczak¹

Institute of Low Temperature and Structure Research, Polish Academy of Sciences, Okólna 2, 50-422 Wrocław, Poland



ARTICLE INFO

Article history:

Received 30 November 2020

Accepted 31 December 2020

Available online 16 January 2021

Keywords:

Zinc(II) phthalocyanine derivatives

Crystal structure

Peripherally octa-substituted Zn(II)

phthalocyanine complexes

DFT and TD DFT

UV-Vis

ABSTRACT

A series of zinc(II) phthalocyanine complexes peripherally octa-substituted by methyl groups and with axially ligated *N*-donor ligands, $\text{Zn}(\text{Me})_8\text{Pc-L}$, where L is pyridine (**4**), 3-methylpyridine (**5**), 3,4-lutidine (**6**) and 3,5-lutidine (**7**), was synthesized. All the $\text{Zn}(\text{Me})_8\text{Pc-L}$ complexes **4–7** were obtained in the crystalline form, suitable for X-ray single crystal analysis. The effect of the peripheral substituents as well as the ligation effect of the axial ligands on the structure were analyzed. In all the here studied zinc(II) phthalocyanine derivatives, the interaction of the metal center with the N atom of the axial ligand results in its displacement by ~ 0.4 Å from the N_4 -isoindole plane of phthalocyaninate macrocycle that adopts a saucer-shaped form. The X-ray geometry and stereochemistry of the zinc(II) phthalocyanine derivatives were compared with that obtained by DFT methods. Analysis of the Hirshfeld's surface shows a reduction of the $\pi\cdots\pi$ interactions with the simultaneous increase of the C–H \cdots N, C–H \cdots N, H \cdots H and C–H \cdots π interactions in the investigated complexes **4–7**. Partial MO energy diagrams and the calculated absorption spectra of the $\text{Zn}(\text{Me})_8\text{Pc-L}$ derivatives **4–7** exhibit a bathochromic shift of the maximum absorption wavelength (λ_{max}) in comparison with the spectrum of $\text{Zn}(\text{Me})_8\text{Pc}$ by about 20 nm. Complexes **4–7** have a strong absorption band in the therapeutic window (600–900 nm) and the HOMO-LUMO energy gap is sufficient to excite the ground state of oxygen and therefore they can be tested as potential photosensitizers for PDT.

© 2021 Elsevier Ltd. All rights reserved.

1. Introduction

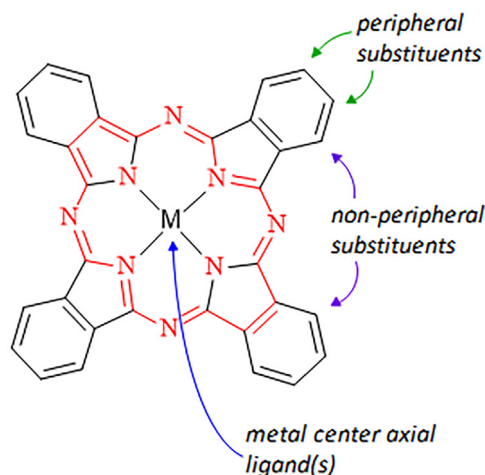
Phthalocyanines (Pcs) composed of four isoindole units connected by azamethine bridges are planar macrocyclic compounds containing an extended 18π electron conjugated aromatic system (Scheme 1) [1]. Due to their fascinating and various properties, as well as their high thermal and chemical stability, they are a very important class of compounds that offer varied and diverse applications. Because of their intense blue-violet colour they were initially used in industry as dyes and pigments [2]. A still increasing interest in phthalocyanines is due to their unique electronic and optical properties [3] as well as unexceptional extraordinary photophysical, photochemical and electrochemical properties [4] that give opportunities for their application as gas sensors [5], solar cells [6], non-linear optics [7], optical data storage devices [8], near-IR imaging agents [9], active matrix displays [10] and organic light-emitting diodes (OLEDs) [11]. Metallophthalocyanines, including zinc phthalocyanine and its derivatives, with low toxicity have confirmed to be promising as photosensitizers for PDT, in

view of their strong intense absorption in the therapeutic window, namely in the red region of visible light [12]. An influential photosensitizer for PDT application should be characterized with a high singlet oxygen generation capacity, high triplet state quantum yields and long triplet life-time. The limited solubility of large planar metallophthalocyanines and their aggregation behavior in biological systems is a very common phenomenon in this family of compounds due to π - π interactions between the molecules with extended π -electron delocalized systems, which decreases their fluorescence quantum yields and shortens their triplet lifetime, and thus reduces their photosensitizing efficiency [13].

Many of these applications are closely related to the solubility of the photosensitizers, which results directly from their structures and the nature of the intermolecular interactions in the solid. The great architectural flexibility of metallophthalocyanines can be exploited to tune the molecular properties in pursuit of optimized features, like as color, aggregation and optical absorption properties. There are several ways to improve their solubility and reduce their ability to aggregate in solutions. One way to improve their solubility is adding steric substituents in the peripheral and/or non-peripheral positions of the phthalocyanine macrocycle. Another way is to modify the metal center complexation by

¹ ORCID: 0000-0001-9826-5821.

E-mail address: j.janczak@intibs.pl



Scheme 1. The ways of possible modifications of metallophthalocyanines, showing in red the 18- π electron aromatic macrocycle.

coordinating additional axial ligand(s). The third way to modify and increase the solubility of MPCs is to use both methods simultaneously, i.e. H-substitution in the Pc ring and axial ligation of the central metal of the MPC macrocycles (Scheme 1). All above mentioned structural modifications of metallophthalocyanines were found to be able to prohibit close self-organization of the macrocycle, even in the solid state, and lead to improvement of their solubility due to decreasing of the π - π interactions between the highly-conjugated 18- π electron aromatic macrocycles.

Several structures of metal(II) phthalocyanines, including ZnPc with various axial ligands, obtained by metal center complexation are reported [14]. This work is aimed at the synthesis and crystallization of modified zinc phthalocyanine derivatives, in which the modification occurs both on the peripheral carbon atoms of the phthalocyanine macrocycle as well as the coordination sphere on the central Zn atom in ZnPc. The influence of both modification effects of ZnPc, i.e. the introduction of methyl group substituents at each peripheral position of the phthalocyanine macrocycle as well as modification of the central zinc atom, on the self-assembly and π - π interactions between the modified macrocyclic rings in the solid state as well as their influence on the solubility have not been studied systematically so far. Trends in the π - π interactions between the investigated peripherally methyl octa-substituted zinc(II) phthalocyanine molecules were analyzed using Hirshfeld surface (HS) and 2D-fingerprint plots. In addition, the influence of such a structural modification of the phthalocyanine core as well as modification of the coordination sphere of the central Zn atom of on the change of the absorption position of the most intense Q band and the molar absorption coefficient was investigated. The experimental results are supported by DFT and TD DFT calculations.

2. Experimental

2.1. Materials and methods

O-xylene, iodine, bromine, chloroform, dimethylformamide, pyridine, 3-methylpyridine, 3,4-lutidine, 3,5-lutidine and the metal salts were obtained from Sigma-Aldrich. All solvents were purified prior to use by standard procedures. Metal salts were kept before syntheses in a vacuum drying oven for 5 h at 110 °C. The composition of the obtained crystals was checked with a Perkin-Elmer 2400 elemental analyzer and with energy dispersive spectroscopy (EDS). EDS spectra were acquired and analyzed using an

EDAX Pegasus XM4 spectrometer with an SDD Apollo 4D detector mounted on a FEI Nova NanoSEM 230 microscope. In addition, the elemental analysis was carried out with a Perkin-Elmer 240 elemental analyzer. A thermogravimetric study (TGA) for the investigated compound was performed over the temperature range 20–300 °C using a Perkin Elmer TGA 4000. The sample weight was ca. 25 mg. The heating speed rate was 5 °C/min. Pure nitrogen gas as a dynamic ambient atmosphere was used. The Fourier transform infrared spectra were recorded between 4000 and 450 cm^{-1} on a Bruker IFS 113 V FTIR in KBr pellets (Fig. S1). Measurements of the UV-Vis spectra were carried out at room temperature using an Agilent UV-Vis/NIR Cary 5000 spectrometer. The UV-Vis spectra were recorded in pyridine ($c = 10^{-6}$ mol/l) and toluene ($c = 5 \times 10^{-7}$ mol/l) solutions. Diffuse Reflectance Spectroscopy (DRS) experiments were conducted on a Cary-Agilent 5000 spectrometer with a Praying Mantis diffuse reflectance attachment. The powder samples were loaded in a holder with a quartz window and were measured in the region 300–1100 nm. A powder Al_2O_3 reflectance standard was used as the baseline. To minimize the effects of regular reflection and particle size, the sample was diluted with a non- or weak absorbing colorless standard of Al_2O_3 . The concentration of the studied $\text{Zn}(\text{Me})_8\text{Pc-L}$ derivatives in the used Al_2O_3 diluent was $\sim 5\%$ by weight. The corresponding diluent was also used as the baseline standard. In addition, the same support was also used as the diluent as well as the standard to examine the effect of the oxide support contribution to the overall DRS spectra. The DRS spectra of the samples were recorded under ambient conditions.

2.2. Synthesis of 1,2-dimethyl-4,5-dibromobenzene (2)

O-xylene (100 mL, 828 mmol) was placed in a 500 mL round-bottom flask and then bromine (96.5 mL, 1.86 mol) was added gradually dropwise over about 3 h, maintaining the temperature around 0 °C (ice bath) and with stirring (magnetic stirrer). The resulting solid cake was then allowed to stand at room temperature for 24 h. The resulting product was dissolved in 500 mL diethyl ether and washed with 300 mL 2-molar KOH and 200 mL deionized water by shaking. The ether solution was dried over anhydrous MgSO_4 , filtered and the organic phase was concentrated on a rotary evaporator to afford a faintly pink coloured oil which solidified upon standing. Recrystallization of the crude product from MeOH gave a white crystalline product in a yield of $\sim 70\%$ (152.7 g, 578.5 mmol), m.p. 88–89 °C. A selected crystal was checked on a single crystal X-ray diffractometer. The lattice parameters obtained were: $a = 9.385(2)$, $b = 7.920(2)$ and $c = 12.616(3)$ Å and $\beta = 109.06(2)^\circ$, which are consistent with the literature data [15]. The purity of the obtained crystalline product was also checked with a powder diffractometer. The experimental X-ray powder pattern is consistent with the calculated one (Fig. S2 in SI).

2.3. Synthesis of 4,5-dimethylphthalonitrile (3)

A mixture of 4,5-dibromoxylene (26.4 g, 0.1 mol) and CuCN (42 g, 0.47 mol) in DMF (200 mL) was refluxed for 6 h. After cooling, the solution was poured into 1 L of a solution of FeCl_3 . The precipitate was filtered off, washed with water and extracted with CHCl_3 (600 mL). The extract was dried with CaCl_2 . The solvent was distilled off on a rotary evaporator and the resulting product was purified by recrystallization from benzene, yielding a light-yellow solid in the crystalline form. The solid 4,5-dimethylphthalonitrile was obtained in a yield of 71% (11.10 g, 71 mmol), m.p. 171–172 °C.

2.4. Synthesis of the zinc phthalocyanine complexes 4–7

A mixture of 4,5-dimethylphthalonitrile **3** (0.2 g, 1.282 mmol) and zinc acetate (0.08 g, 0.372 mmol) in a glass ampoule was covered with 10 mL pyridine (3-mepy, 3,4-lutidine or 3,5-lutidine) and a few drops of DBU as a catalyst. Next the ampoule was degassed and sealed under reduced pressure. The ampoule was heated at a temperature of about 10 °C below the boiling point of pyridine or its corresponding derivative for about 20 h. After such processes, well-developed single crystals suitable for single-crystal X-ray analysis were obtained. The crystals were separated by filtration, washed with acetone and diethyl ether, and dried in air.

Zinc(II)(pyridine)-2,3,9,10,16,17,23,24-octamethylphthalocyanine (**4**). Yield: 40.5% (0.100 g, 0.130 mmol). Analysis found: Zn, 8.42; C, 70.55; N, 16.44; H, 4.59%; calculated for $C_{40}H_{32}N_8Zn$ (C_5H_5N): Zn, 8.50; C, 70.26; N, 16.39; H, 4.85%. IR/KBr (cm^{-1}): 3400w, 3287w, 2915w, 2216w, 1615 m, 1564w, 1517 s, 1498 s, 1446 m, 1394 m, 1372 m, 1330w, 1303 s, 1181w, 1134w, 1101vs, 1024 s, 1010vs, 878 m, 838 m, 781w, 775 s, 730w, 689 s.

Zinc(II)(3-methylpyridine)-2,3,9,10,16,17,23,24-octamethylphthalocyanine (**5**). Yield: 37.7% (0.095 g, 0.121 mmol). Analysis found: Zn, 8.30; C, 70.78; N, 16.00; H, 4.92%; calculated for $C_{40}H_{32}N_8Zn(C_6H_7N)$: Zn, 8.35; C, 70.54; N, 16.09; H, 5.02%. IR/KBr (cm^{-1}): 3394w, 3344w, 2360w, 2336w, 1617w, 1562w, 1486 m; 1450, 1399 m, 1378 m, 1308 s, 1239 m 1202w, 1178 m, 1132w, 1099vs, 1020 s, 988 m, 877 m, 855 m, 804w, 790w, 749 s, 711 s, 668 m, 646 m, 572w, 502w.

Zinc(II)(3,4-dimethylpyridine)-2,3,9,10,16,17,23,24-octamethylphthalocyanine (**6**). Yield: 38.3% (0.098 g, 0.123 mmol). Analysis found: Zn, 8.10; C, 71.08; N, 15.68; H, 5.14%; calculated for $C_{40}H_{32}N_8Zn(C_7H_9N)$: Zn, 8.20; C, 70.81; N, 15.81; H, 5.18%. IR/KBr (cm^{-1}): 3382w, 3338w, 1614 m, 1485 s, 1458 m, 1398 m, 1374w, 1332 m, 1308 s, 1240 m, 1203 m, 1174w, 1133w, 1098vs, 1018 s, 988 m, 874 m, 857 m, 824w, 805w, 748 s, 714 s, 610w, 572w, 523w, 502w.

Zinc(II)(3,5-dimethylpyridine)-2,3,9,10,16,17,23,24-octamethylphthalocyanine (**7**). Yield: 38.6% (0.099 g, 0.124 mmol). Analysis found: Zn, 8.08; C, 61.12; N, 15.66; H, 5.145%; calculated for $C_{40}H_{32}N_8Zn(C_7H_9N)$: Zn, 8.20; C, 70.81; N, 15.81; H, 5.18%. IR/KBr (cm^{-1}): 3380w, 3336w, 1615 m, 1487 s, 1458 m, 1399 m, 1376w, 1334 m, 1304 s, 1240w, 1173w, 1134w, 1098vs, 1019 s, 987 m, 878 m, 858 m, 804 m, 748 s, 714 s, 667w, 574w, 548w, 502 m.

2.5. X-ray single crystal measurement

The obtained single crystals of **4–7** were used for data collection on a four-circle KUMA KM4 diffractometer equipped with a two-dimensional CCD area detector. Graphite monochromatized Mo-K α radiation ($\lambda = 0.71073 \text{ \AA}$) and the ω -scan technique ($\Delta\omega = 1^\circ$) were used for data collection. Lattice parameters were refined by least-squares methods on all reflection positions. One image was monitored as a standard after every 40 images for a control of the stability of the crystal. Data collection and reduction along with absorption correction were performed using the CrysAlis software package [16]. The structures were solved by direct methods using *SHELXT* [17], giving positions of almost all non-hydrogen atoms. Initially, the structures were refined using *SHELXL-2018* [18] with anisotropic thermal displacement parameters. Hydrogen atoms of the phthalocyanine moiety as well as of the axial ligands were refined as rigid. Visualizations of the structures were made with the Diamond 3.0 program [19]. Details of the data collection parameters, crystallographic data and final agreement parameters are collected in Table 1.

2.6. Powder X-ray diffraction (PXRD)

The purity of the obtained peripherally octamethyl zinc(II) phthalocyanines with various axial substituents (**4–7**) were checked by powder X-ray diffraction on a PANanalytical X'Pert diffractometer equipped with a Cu-K α radiation source ($\lambda = 1.54182 \text{ \AA}$). The diffraction data were recorded in the range 5–50 ° at room temperature. The powder diffraction patterns of **4–7**, together with the simulated ones, are included in the [supporting information \(Fig. S3\)](#).

2.7. Hirshfeld surface analysis

Hirshfeld surface analysis and 2D fingerprint plots, as well as percentage contributions for various intermolecular contacts in the investigated crystals, were calculated using the Crystal Explorer Ver. 3.1 program package [20].

2.8. Theoretical calculations

Molecular orbital calculations with full geometry optimization of the zinc phthalocyanine complexes **4–7** were performed with the Gaussian16 program package [21]. All calculations were carried out using the DFT method (Becke3-Lee-Yang-Parr exchange correlation functional B3LYP) [22] with the 6-31G basis set [23], assuming the geometry resulting from the X-ray diffraction study as the starting structures. As convergence criterions, the threshold limits of 0.00025 and 0.0012 a.u. were applied for the maximum force and the displacement, respectively. The three-dimensional molecular electrostatic potential (3D MESP) maps were obtained on the basis of the DFT (B3LYP/6-31G) optimization. The calculated 3D MESP was mapped onto the total electron density isosurface (0.008 e \AA^{-3}) for each molecule. The colour code of the MESP maps is in the range -0.05 (red) to 0.05 e \AA^{-1} (blue). After the geometry optimization, time-dependent (TD) DFT calculations [24] were performed to evaluate the absorption spectrum employing the same level and basis sets. All stationary points were optimized without any symmetry assumptions and characterized by normal coordinate analysis at the same level of theory.

3. Results and discussion

3.1. Synthesis

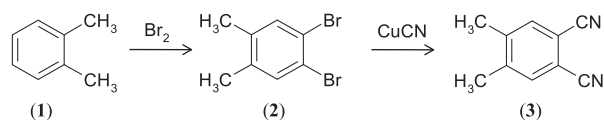
4,5-Dimethylphthalonitrile was obtained from *o*-xylene in a two-step reaction using standard procedures [25], as shown in [Scheme 2](#). The octa-substituted zinc phthalocyanine complexes **4–7** were prepared starting from 4,5-dimethylphthalonitrile **3** and zinc acetate, as shown in [Scheme 3](#). The reaction was carried out by the solvothermal method using a suitable solvent that also played the role of an axial ligand as well as the role of the crystallization medium. In addition, a few drops of 1,8-diaza[5.4.0]bicycloundec-7-ene (DBU) were added to the reaction mixture as a catalyst. The solvothermal reactions were carried out in glass ampoules under reduced pressure at about 10 °C below the boiling point of respective solvents (pyridine or its corresponding derivative) for about 20 h and then they were cooled to room temperature. Under the solvothermal conditions, the tetramerization of nitrile **3** with the simultaneous incorporation of the Zn^{2+} ion into the central hole of the formed octamethyl-substituted phthalocyaninate(2-) macrocycle takes place. The formed octamethyl substituted zinc phthalocyanine then interacts with pyridine or its respective derivative yielding the axially ligated complexes **4–7**. The direct thermal reaction of 4,5-dimethylphthalonitrile with zinc in the powdered form without pyridine or other solvents was also

Table 1
Crystal data and final refinement parameters.

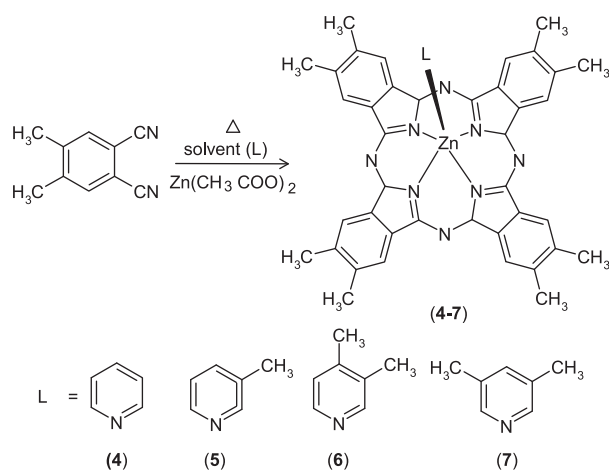
	4	5	6	7
Formula	C ₄₅ H ₃₇ N ₉ Zn	C ₄₆ H ₃₉ N ₉ Zn	C ₄₇ H ₄₁ N ₉ Zn	C ₄₇ H ₄₁ N ₉ Zn
Molecular weight	769.20	783.23	797.26	797.26
Crystal system	triclinic	triclinic	triclinic	triclinic
Space group	<i>P</i> -1	<i>P</i> -1	<i>P</i> -1	<i>P</i> -1
<i>a</i> (Å)	11.6888(5)	11.9300(10)	11.9023(7)	12.1688(11)
<i>b</i> (Å)	12.6385(6)	12.3287(12)	12.4117(8)	12.1848(12)
<i>c</i> (Å)	13.3262(7)	14.2326(15)	14.2480(9)	14.5816(14)
α (°)	99.113(4)	102.251(6)	102.310(7)	106.139(8)
β (°)	104.705(4)	109.408(8)	108.180(10)	102.340(8)
γ (°)	102.214(4)	102.738(9)	101.440(10)	102.526(8)
<i>V</i> (Å ³)	1813.64(16)	1830.7(3)	1872.6(2)	1939.0(3)
<i>Z</i>	2	2	2	2
<i>F</i> (000)	800	816	832	832
Temperature (K)	295(2)	295(2)	295(2)	295(2)
<i>D</i> _{calc} [g cm ⁻³]	1.409	1.421	1.414	1.366
μ (mm ⁻¹)	0.725	0.720	0.705	0.681
Crystal size (mm ³)	0.21 × 0.19 × 0.15	0.34 × 0.21 × 0.15	0.29 × 0.27 × 0.14	0.28 × 0.24 × 0.15
Abs. correction	multi-scan	multi-scan	multi-scan	multi-scan
<i>T</i> _{min} / <i>T</i> _{max}	0.9324 / 1.000	0.8947 / 1.000	0.9262 / 1.000	0.9352 / 1.000
Total / Unique / Obs reffs	25,430 / 9175 / 4922	25,556 / 9159 / 6597	24,055 / 8505 / 4549	26,930 / 9644 / 4950
<i>R</i> _{int}	0.0748	0.0290	0.0725	0.0813
<i>R</i> [<i>F</i> ² > 2σ(<i>F</i> ²)] ^a	0.0638	0.0402	0.0740	0.0660
w <i>R</i> [<i>F</i> ² all reffs] ^b	0.1015	0.0915	0.1213	0.1012
<i>S</i>	1.002	1.047	1.062	1.010
$\Delta\rho_{\max}$, $\Delta\rho_{\min}$ (e Å ⁻³)	0.419, -0.416	0.314, -0.361	0.508, -0.420	0.362, -0.411
CCDC No.	2027869	2027870	2027871	2027872

^a $R = \sum ||F_o| - |F_c|| / \sum F_o$.

^b $wR = (\sum [w(F_o^2 - F_c^2)^2] / \sum wF_o^4)^{1/2}$; $w^{-1} = \sigma^2(F_o^2) + (aP)^2 + bP$ where $P = (F_o^2 + 2F_c^2)/3$. The *a* and *b* parameters are 0.0294 and 0.0027 for **4**, 0.0236 and 1.5630 for **5**, 0.0024 and 3.8995 for **6**, and 0.0083 and 1.9641 for **7**.



Scheme 2. Synthetic route to 3,5-dimethylphthalonitrile.



Scheme 3. Synthetic strategy used to prepare the complexes **4-7**.

performed by the procedure used for the synthesis of normal unsubstituted MPcs, described elsewhere [26], however all attempts resulted in octamethyl substituted zinc phthalocyanine in the powdered form. So, the pyridine or its respective derivatives present in the reaction played a role not only as a reactive medium but also as an axial ligand due to their coordination abilities, and additionally as a medium for crystallization of the formed ZnPc-complexes.

For a better understanding of the reaction formation of the zinc phthalocyanine derivatives during the solvothermal processes as well as the nature of the interaction between the reacting molecules, three-dimensional molecular electrostatic potentials have been calculated [27]. The molecular electrostatic potential (MESP) is related to the electronic density in a molecule and is a very useful tool in determining sites for electrophilic and nucleophilic reactions as well as for intermolecular interactions and the organization of molecules in the solid-state [28]. The three-dimensional MESP maps of 4,5-dimethylphthalonitrile, that undergoes cyclotetramerization in the presence of Zn²⁺ ions with the formation of the zinc phthalocyanine derivative, as well as for the reaction solvent molecules (pyridine, 3-picoline, 3,4-lutidine or 3,5-lutidine) and the final product molecules were calculated (Fig. 1). Looking at the 3D MESP maps, it can be seen that the formed octamethyl-substituted zinc phthalocyanine, with a positive EP about the central Zn(II) ion on both sides of the macrocyclic Pc ring, in a solution of pyridine or its corresponding derivatives can interact with the ring nitrogen atom of the solvent, which has a negative EP. As a result of this interaction, an axial Zn-N donor-acceptor bond is formed. The MESP maps calculated for the reaction product molecules, i.e. the octamethyl-substituted zinc phthalocyanines, are helpful in understanding the process of their nucleation and crystal growth.

3.2. Thermal properties

In order to determine the thermal stability of the obtained compounds in the crystalline form, thermal analysis was carried out on samples of about 25 mg, with a heating rate of 5 °C/min. Thermogravimetric analyses of the investigated compounds **4-7** are illustrated in Fig. 2. All the investigated complexes are relatively very stable and show one step of weight loss during heating. The weight loss is related to the breaking of the axial coordination Zn-N bond and the release of the axial ligand (pyridine – **4**, 3-picoline – **5**, 3,4-lutidine – **6** and 3,5-lutidine – **7**) at a respective temperature

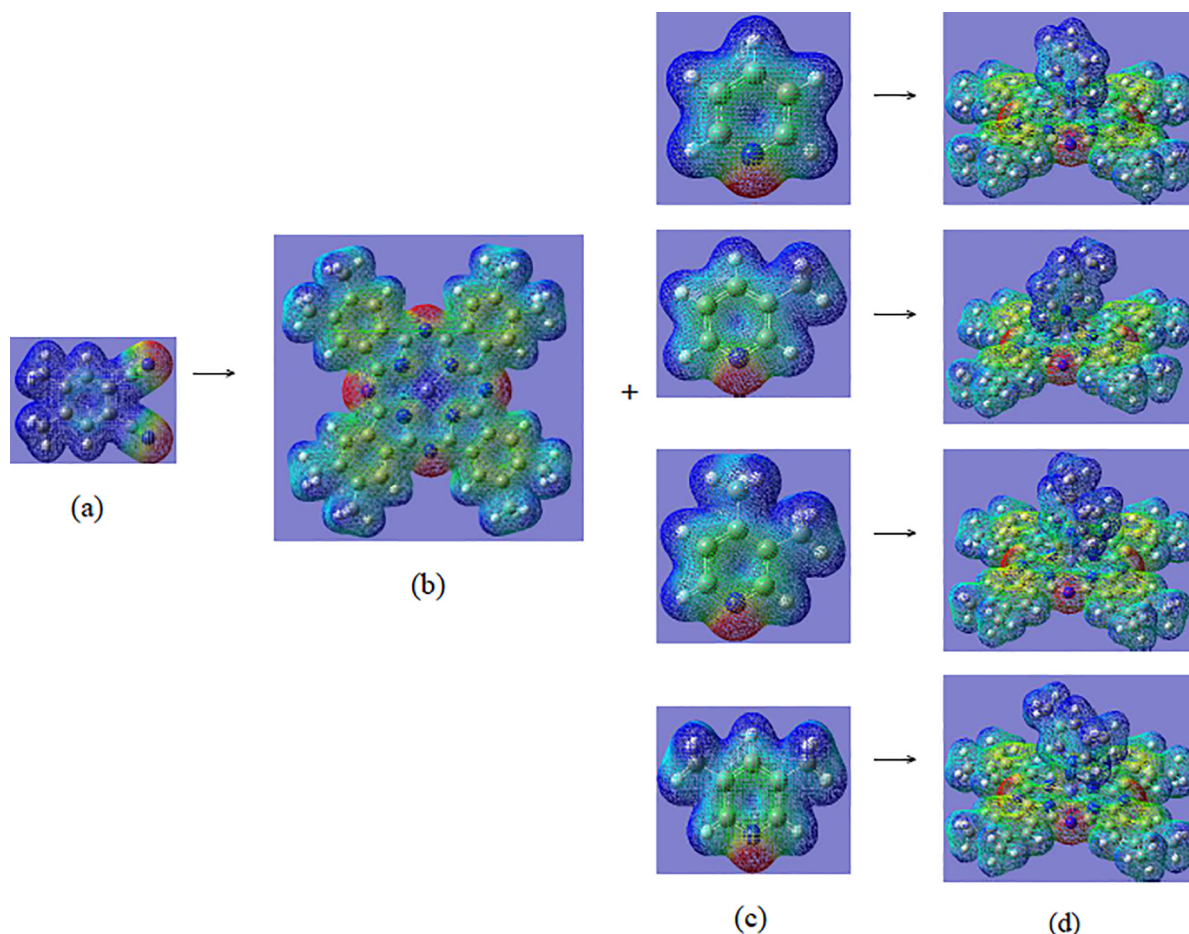


Fig. 1. The calculated 3D MESP is mapped onto the total electron density isosurface ($0.008 \text{ e} \text{ \AA}^{-3}$) for 4,5-dimethylphthalonitrile (a), the octa-substituted $\text{Zn}[(\text{Me})_8\text{-Pc}]$ derivative (b), solvent molecules (L): pyridine, 3-methylpyridine, 3,4-lutidine and 3,5-lutidine (c) and the final products of $\text{Zn}[(\text{Me})_8\text{-Pc}]L$ (d). The colour code of the MESP is in the range -0.05 (red) to $0.05 \text{ e} \text{ \AA}^{-1}$ (blue). ((Colour online.))

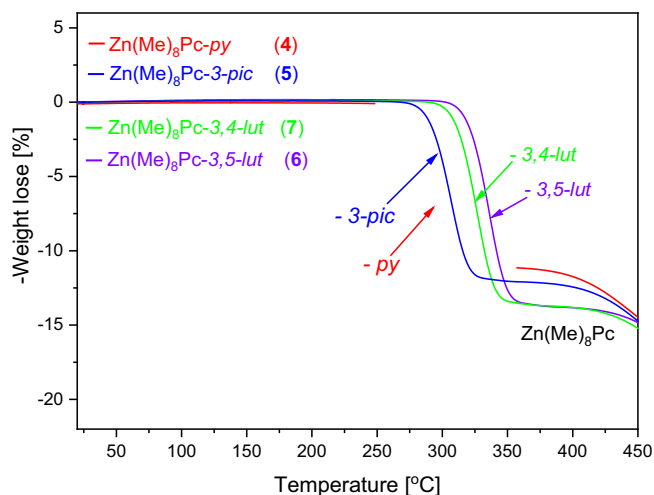


Fig. 2. Thermogram for $\text{Zn}(\text{Me})_8\text{Pc-py}$ (4), $\text{Zn}(\text{Me})_8\text{Pc-3-pic}$ (5), $\text{Zn}(\text{Me})_8\text{Pc-3,4-lut}$ (6) and $\text{Zn}(\text{Me})_8\text{Pc-3,5-lut}$ (7).

which correlates with the axial ligand binding force, intermolecular interactions and the crystal packing. The weight losses are 11.45 and 12.00% for **4** and **5**, respectively, and the weight loss for complexes **6** and **7** is almost the same and equal to 13.50%. The weight losses are in agreement with the calculated values:

11.33% for $\text{Zn}(\text{Me})_8\text{Pc-py}$ (**4**), 11.89% for $\text{Zn}(\text{Me})_8\text{Pc-3-pic}$ (**5**) and 13.44% for octamethyl-substituted zinc phthalocyanine ligated by 3,4-lutidine (**6**) and 3,5-lutidine (**7**). Finally, the sample gives the octamethyl-substituted zinc phthalocyanine $\text{Zn}(\text{Me})_8\text{Pc}$ that undergoes sublimation above 400–450 °C.

3.3. Structural characterization

Single crystals suitable for X-ray diffraction of all the $\text{Zn}(\text{Me})_8\text{Pc-L}$ derivatives ($L = \text{pyridine, 3-picoline, 3,4-lutidine and 3,5-lutidine}$) were obtained in a one-step method by the direct reaction of 4,5-dimethylphthalonitrile with $\text{Zn}(\text{CH}_3\text{COO})_2$ in the respective solvents, which play the role of not only as the axial ligation ligand by also the crystallization medium. All the $\text{Zn}(\text{Me})_8\text{Pc-L}$ derivatives crystallize in the centrosymmetric space group of the triclinic system with two molecules per unit cell (Table 1). The asymmetric unit of the crystals consists of one $\text{Zn}(\text{Me})_8\text{Pc-L}$ molecule (Fig. 3).

The $\text{Zn}(\text{Me})_8\text{Pc-L}$ molecules exhibit a similar conformation, in which the divalent zinc ion is coordinated with the four isoindole nitrogen atoms of the octamethyl-substituted phthalocyaninate (2-) macrocycle and, in addition, with the nitrogen atom of the axial ligand (L). Thus, the coordination polyhedron of the zinc(II) ion in all the complexes exhibits a slightly distorted square pyramid. However, due to the interaction between the zinc(II) center of $\text{Zn}(\text{Me})_8\text{Pc}$ and the lone electron pair on the sp^2 orbital of the N atom of pyridine or its derivatives, with the formation of an axial Zn–N bond, the divalent central zinc(II) ion does not lie in the cen-

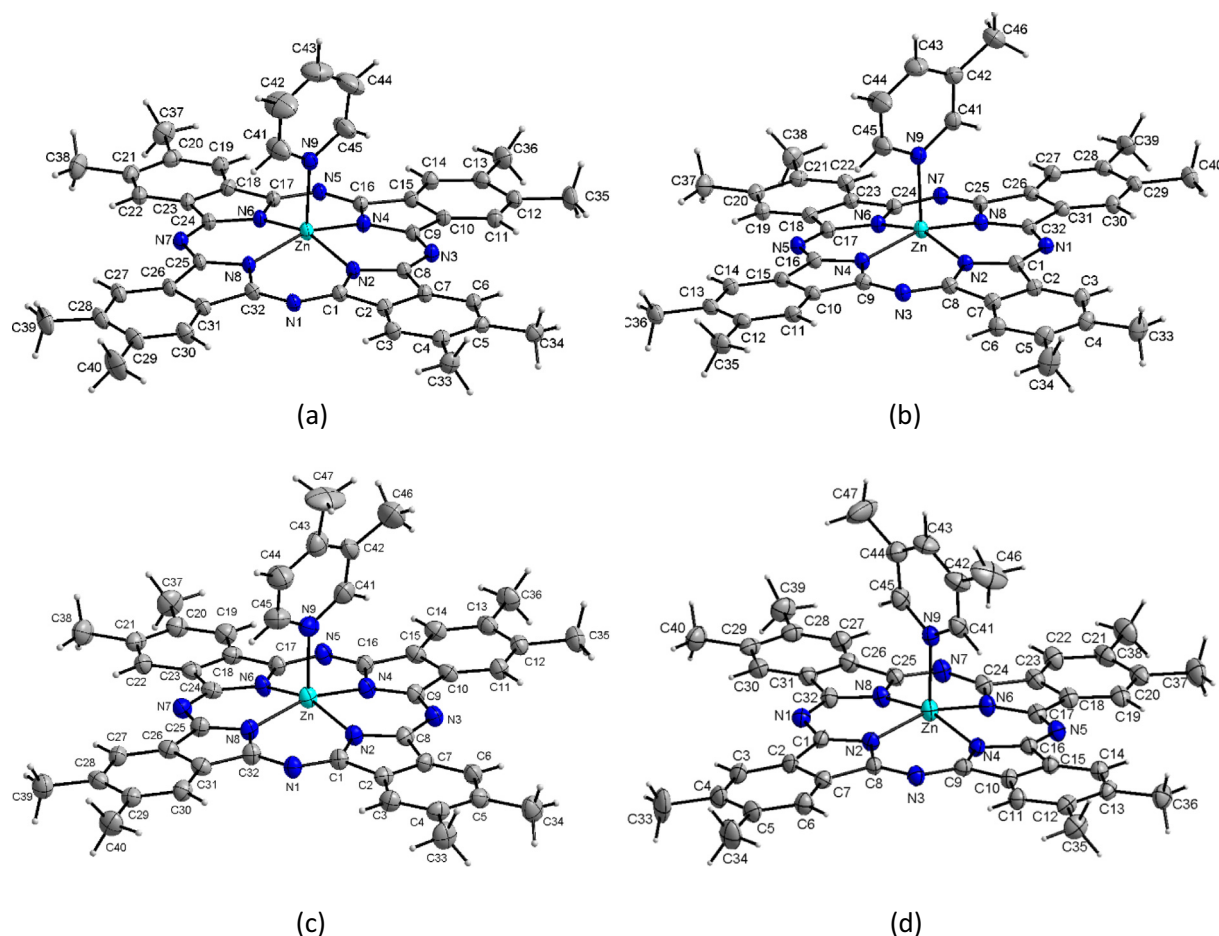


Fig. 3. View of the asymmetric unit of **4** (a), **5** (b), **6** (c) and **7** (d).

tral hole of $(\text{Me})_8\text{Pc}^{2-}$, but is deviated by $0.38(2) \text{ \AA}$ from the plane defined by the four isoindole N atoms of the $(\text{Me})_8\text{Pc}^{2-}$ macrocycle toward to the N atom of the axial ligand. The deviation of the Zn (II) ion from the N_4 -isoindole plane is very similar in all the Zn $(\text{Me})_8\text{Pc-L}$ molecules (Table 2), however, a tendency to reduce the Zn deviation from the ring plane going from the pyridine complex ($0.397(3) \text{ \AA}$) to 3-picoline ($0.387(3) \text{ \AA}$) and then to 3,4-lutidine ($0.372(3) \text{ \AA}$) and 3,5-lutidine ($0.365(4) \text{ \AA}$) is noticed. This tendency correlates well with the coordination properties and the basicity of the ligands: $pK_b = 8.77$ for pyridine, 8.32 for 3-picoline, 7.85 for 3,5-lutidine and 7.54 for 3,4-lutidine [29]. The deformation of the $(\text{Me})_8\text{Pc}^{2-}$ ring form planarity can be determined by the inclination of the four planar isoindole units to the N_4 -plane and is ranges from $0.91(3)$ to $6.00(3)$, $1.80(3)$ to $7.50(3)$, $2.011(3)$ to $4.51(3)$ and $1.10(3)$ to $8.50(3)^\circ$ in **4**, **5**, **6** and **7**, respectively (Table 2). The four equatorial Zn–N bonds with the $(\text{Me})_8\text{Pc}^{2-}$ macrocycle are very similar in all the molecules, however, they are still slightly shorter than the axial bond linking the central zinc ion to the axial pyridine or its derivative ligands (Table 2). A search of the Cambridge Structural Database (CSD, Version 5.41) shows a similar correlation between the equatorial and axial Zn–N bonds observed in several $4 + 1$ -coordinated ZnPc-derivatives that have been structurally characterized [30].

The orientation of the axial ligand in **4**, **5**, **6** and **7** ligated to the central Zn(II) ion in relation to the octamethyl-substituted phthalocyaninate(2-) macrocycle is well described by the $\text{N}_2\text{—Zn—N}_9\text{—C}_{45}$ torsion angle. Rotation of the ligands around the axial Zn–N₉ bond would reduce the steric hindrance effect, i.e. the non-bonding distances between the hydrogen atoms in the *ortho* posi-

Table 2
Selected geometrical parameters for $\text{Zn}(\text{Me})_8\text{Pc-py}$ (**4**) (\AA , $^\circ$).

	X-ray	DFT
Zn–N2	2.018 (2)	2.045
Zn–N4	2.018 (2)	2.043
Zn–N6	2.027 (2)	2.045
Zn–N8	2.019 (2)	2.045
Zn–N9	2.166 (2)	2.215
N2–Zn–N9	97.52 (9)	101.86
N4–Zn–N9	101.61 (9)	101.36
N6–Zn–N9	105.44 (9)	101.88
N8–Zn–N9	100.79 (9)	101.36
N2–Zn–N9–C45	87.08 (3)	90.00
Deviation of Zn from the N_4 -isoindole plane	0.397 (3)	0.412
Dihedral angle		
N_4 -isoindole/N2,C1–C8	0.91 (3)	4.49
N_4 -isoindole/N4,C9–C16	4.70 (3)	6.01
N_4 -isoindole/N6,C17–C24	2.51 (3)	4.69
N_4 -isoindole/N8,C25–C32	6.00 (3)	6.01

tion to the *N*-pyridine or its derivatives atom of the axial molecules and the atoms of the octamethyl-substituted phthalocyaninate(2-) ring. In particular, if the rotation angle is equal 0 or 90° , the planar axial molecule is parallel to the Zn–N_{iso} bond. The second orientation, with a rotation angle of 45° (or the equivalent 135°) makes the axial ligand parallel to the Zn–N_{axa} bond. Both orientations of the axial ligands are preferred by the electrostatic interaction between the positively polarized hydrogen atoms from the *ortho* position of the ligand and the indole or azamethine nitrogen atoms

of the macrocycle with opposite polarization (see Fig. 1). However, in the crystals, due to intermolecular interactions and crystal packing forces, the rotation of the axial ligands around the axial Zn–N9 bond is slightly deviated from the ideal torsion angle mentioned above (see Tables 2–5). The non-bonding distances between the *ortho*-H atom of the axial pyridine derivatives and the *N*-isoindole atoms of the macrocycle are 2.763 and 2.882 Å in **4**, 2.660 and 2.864 Å in **5**, 2.669 and 2.775 Å in **6** and 2.711 and 2.734 Å in **7**.

In the crystal structure, the molecules interact with each other mainly through H...H dispersion and van der Waals forces. The inversion related molecules in each crystal are arranged in face-to-face dimeric structures with weak $\pi \cdots \pi$ interactions between partially overlapped macrocycles with a distance of ~ 3.65 to ~ 4.22 Å (Cg–Cg (Cg = centrum gravity) of the peripheral six membered rings of the macrocycle) and C–H... π with H...Cg distances of ~ 3.25 to ~ 3.55 Å (Fig. S4), whereas the face-to-face dimeric structures are weakly interacting since the distance between the back-to-back and partially overlapped macrocycles is ~ 3.35 Å (Fig. S5). The $\pi \cdots \pi$ interactions between the partially overlapping saucer-shaped macrocycles in crystals **4–7** are less effective compared to the $\pi \cdots \pi$ interactions in the normal ZnPc crystal. The interaction between the octamethyl-substituted phthalocyaninate(2-) macrocycles in the studied crystals **4–7**, the crystal stability, as well as the relationships between the intermolecular interactions in the crystals and their solubility are discussed in detail in the next paragraph, based on Hirshfeld surface analysis.

3.4. Hirshfeld surface analysis

The Hirshfeld surface (HS) [31] and the analysis of 2D fingerprint plots [32] are good tools to illustrate the interactions between crystal-forming components and can also be useful in explaining the solubility of the compounds studied. The HS not only allows for qualitative analysis of the intermolecular interactions in the crystal, but also allows for quantitative analysis, i.e. it allows the calculation of the contributions of individual types of interactions between the molecules constituting the crystal-building units. To get more detail in the interactions between the octamethyl-substituted zinc phthalocyanine derivative Zn(Me)₈Pc-*L* molecules building the crystals, the HS mapped with d_{norm} [33] and the 2D fingerprint plots were calculated for the whole Zn(Me)₈Pc-*L* molecules of **4–7** (Fig. 4). In the HS, the d_e value corresponds to the distance between the external atom and the surface, and the d_i value corresponds to the distance between the internal atom and the surface. The different interactions between the molecules are related to different colours in the HS. The red areas in the HS correspond to contact distances between atoms inside and outside the surface, and they are smaller than the sum of the respective van der Waals radii. Blue and white areas represent distances that are longer than and equal to the sum of the respective van der Waals radii, respectively.

On the Hirshfeld surface mapped with d_{norm} there are slightly visible red spots originating from the intermolecular C–H...N and C–H...C interactions (Fig. 4, left), whereas on the HS mapped with d_e broad orange-yellow depressions are visible (Fig. 4, middle). The 2D fingerprint plots for complexes **4–7** (Fig. 4, right) provide a concise summary, illustrating the intermolecular interactions occurring in these crystals.

The intermolecular C–H...N / C–H...C or N...H–C / C...H–C interactions are clearly visible as donor and acceptor spikes on the 2D fingerprint charts (Fig. 4, right). The contributions of the C–H...N / N...H–C and C–H...C / C...H–C interactions in the Hirshfeld surface for these complexes are 10.9 and 26.7% in Zn(Me)₈Pc-Py (**4**), 10.3 and 25.0% in Zn(Me)₈Pc-3-Pic (**5**), 9.9 and 24.9% in Zn(Me)₈Pc-3,4-Lut (**6**) and 10.0 and 24.7% in Zn(Me)₈Pc-3,5-Lut (**7**). However,

Table 3
Selected geometrical parameters for Zn(Me)₈Pc-3-pic (**5**) (Å, °).

	X-ray	DFT
Zn–N2	2.0172 (17)	2.046
Zn–N4	2.0252 (17)	2.044
Zn–N6	2.0186 (17)	2.046
Zn–N8	2.0137 (17)	2.043
Zn–N9	2.1761 (19)	2.210
N2–Zn–N9	98.59 (7)	102.02
N4–Zn–N9	99.63 (7)	101.36
N6–Zn–N9	104.99 (7)	102.03
N8–Zn–N9	100.96 (7)	101.75
N2–Zn–N9–C45	89.23 (3)	90.00
Deviation of Zn from the N ₄ -isoindole plane	0.387 (3)	0.440
Dihedral angle		
N ₄ -isoindole/N2,C1-C8	7.50 (3)	4.29
N ₄ -isoindole/N4,C9-C16	2.61 (3)	4.69
N ₄ -isoindole/N6,C17-C24	2.41 (3)	4.69
N ₄ -isoindole/N8,C25-C32	1.80 (3)	4.60

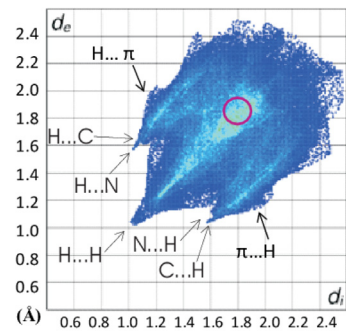
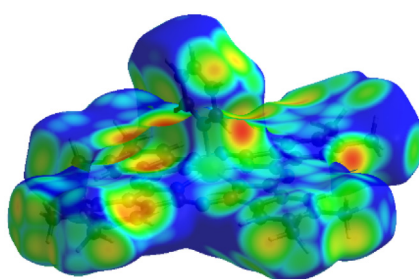
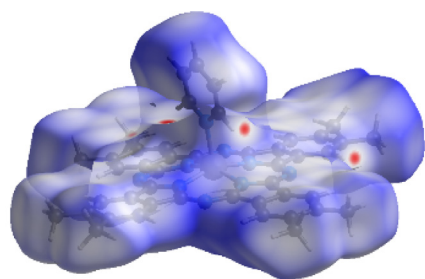
Table 4
Selected geometrical parameters for Zn(Me)₈Pc-3,4-lut (**6**) (Å, °).

	X-ray	DFT
Zn–N2	2.016 (3)	2.048
Zn–N4	2.017 (3)	2.046
Zn–N6	2.009 (3)	2.048
Zn–N8	2.012 (3)	2.045
Zn–N9	2.148 (4)	2.197
N2–Zn–N9	97.52 (13)	102.31
N4–Zn–N9	100.83 (14)	101.76
N6–Zn–N9	105.04 (13)	102.31
N8–Zn–N9	99.17 (14)	101.86
N2–Zn–N9–C45	85.29 (3)	90.00
Deviation of Zn from the N ₄ -isoindole plane	0.372 (3)	0.428
Dihedral angle		
N ₄ -isoindole/N2,C1-C8	4.51 (3)	4.71
N ₄ -isoindole/N4,C9-C16	2.51 (3)	5.99
N ₄ -isoindole/N6,C17-C24	2.01 (3)	4.71
N ₄ -isoindole/N8,C25-C32	3.70 (3)	5.99

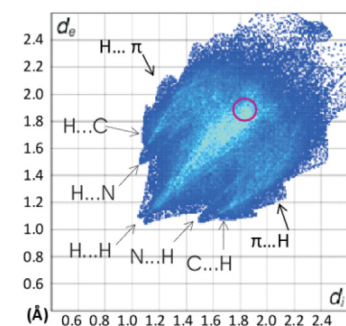
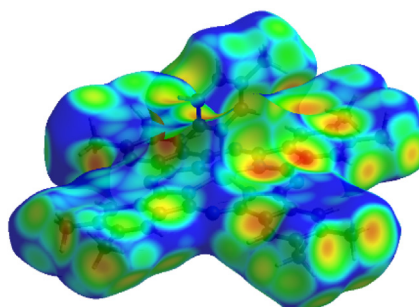
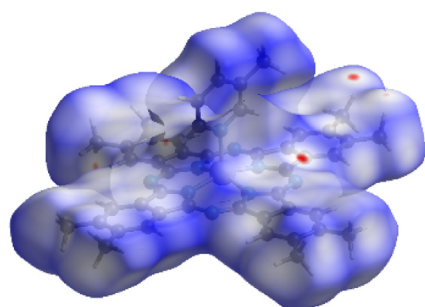
Table 5
Selected geometrical parameters for Zn(Me)₈Pc-3,5-lut (**7**) (Å, °).

	X-ray	DFT
Zn–N2	2.020 (3)	2.047
Zn–N4	2.013 (3)	2.045
Zn–N6	2.020 (3)	2.047
Zn–N8	2.020 (3)	2.045
Zn–N9	2.157 (3)	2.203
N2–Zn–N9	99.68 (10)	102.22
N4–Zn–N9	99.37 (10)	101.77
N6–Zn–N9	104.44 (10)	102.20
N8–Zn–N9	100.14 (11)	101.77
N2–Zn–N9–C45	84.08 (4)	90.00
Deviation of Zn from the N ₄ -isoindole plane	0.365 (4)	0.425
Dihedral angle		
N ₄ -isoindole/N2,C1-C8	8.50 (3)	4.40
N ₄ -isoindole/N4,C9-C16	3.21 (3)	5.70
N ₄ -isoindole/N6,C17-C24	1.31 (3)	4.40
N ₄ -isoindole/N8,C25-C32	1.10 (3)	5.70

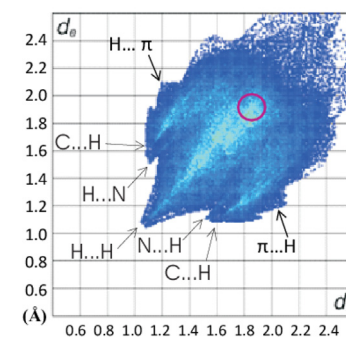
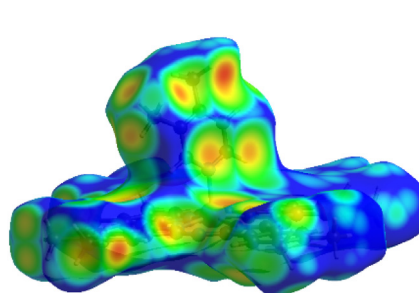
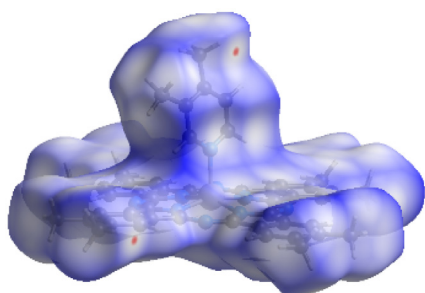
the main contribution in the Hirshfeld surface of these complexes represents H...H dispersive forces. The contributions of the H...H dispersive forces in the HS of these complexes are 53.1% in **4**, 55.1% in **5**, 56.2% in **6** and 57.0% in **7**. The two-dimensional fingerprint plot for these complexes (Fig. 4, right) shows an exceptionally short H...H contact with $d_e = d_i \approx 1.02$ Å (i.e. an H...H separation of 2.04 Å) in the crystal of **4**, whereas for the crystals **5–7** the H...H



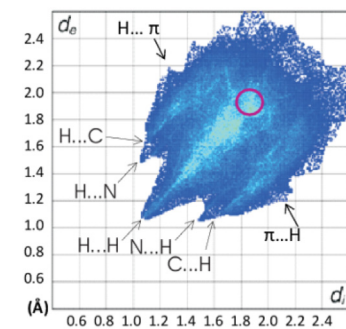
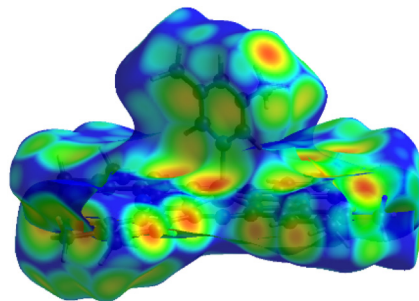
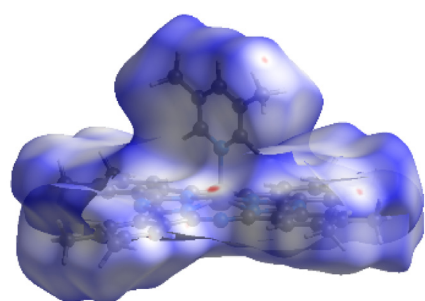
(a)



(b)



(c)



(d)

Fig. 4. Hirshfeld surface mapped with d_{norm} over the range -0.10 to 1.50 (left), with d_e over the range 1.00 to 2.00 (middle) and the two-dimensional fingerprint plots (right) for the molecules of **4** (a), **5** (b), **6** (c) and **7** (d).

contacts are slightly longer, $d_e = d_i \approx 1.07 \text{ \AA}$ (i.e. an H...H separation of *c.a.* 2.14 Å). The contribution of the H...H dispersive forces in the HS of these complexes in crystals **4–7** is about 1/3 greater than that in the normal ZnPc crystal (see Fig. 5). The C...C contact resulting from $\pi\cdots\pi$ stacking interactions appears in normal unsubstituted ZnPc [34] on the diagonal of the fingerprint plots (i.e. where $d_e = d_i$), beginning near the C-atom van der Waals radius of 1.7 Å [35]. In the investigated complexes **4–7**, due to the steric hindrance of the axial ligands as well as due to the octamethyl-substituted Pc-macrocycle and the shift of the macrocycles, each other C...C contact resulting from $\pi\cdots\pi$ interactions is significantly longer and appears on the diagonal of the fingerprint plots at $d_e = d_i$ above 1.8–1.9 Å (red circle in the Fig. 4, right). The contribution in the Hirshfeld surface of the C...C contact resulting from $\pi\cdots\pi$ interactions in the investigated complexes **4–7** of 3–4% is significantly lower in comparison to that in the normal unsubstituted ZnPc complex of ~ 22%, with strong $\pi\cdots\pi$ interactions resulting from the sum of C...C and C...N/N...C intermolecular interactions [34]. The C—H... π interactions in the investigated complexes manifest themselves on the Hirshfeld surface. McKinnon et al. previously have noted that the shape of the surface clearly reflects this contact [36]. The map of the shape index shows these depressions as orange regions with a concave curvature on both sides of the macrocycle, while the C—H donor regions have exactly the opposite curvature and have the opposite shape index and are blue (Fig. 4, middle). The subtle differences of the complementary regions with different colours on the shape index surface are characteristic of any regions of the surface that come into contact with each other and these are observed for the complexes, slightly visible as the 'wings' on the two-dimensional fingerprint plots (Fig. 4, right), and their location depends on the C—H... π distances (see Fig. S4, H...Cg of ~ 3.25 to ~ 3.55 Å). The contribution of the C—H... π interactions to the Hirshfeld surface for the complexes **4–7** is relatively low and does not exceed 5–6%. The contribution of the main intermolecular interactions in the crystals **4–7** is illustrated in Fig. 5, whereas the deconvolution of the 2D-fingerprint plots for individual types of interactions is given in Figs. S5–S8 (SI).

Looking at these results in more detail, it should be stated that although the axial ligand, as a steric hindrance barrier, significantly reduces the stacking effect resulting from the $\pi\cdots\pi$ interactions rel-

ative to unsubstituted normal zinc phthalocyanine (over 4 times), it only improves their solubility relative to normal ZnPc by about 30%. Analysis of the Hirshfeld surface shows that the reduction of the $\pi\cdots\pi$ interactions with the simultaneous increase of the C—H...N, C—H...N, H...H and C—H... π interactions in the investigated complexes **4–7** is the main reason for the relatively small increase in solubility relative to the normal unsubstituted ZnPc.

3.5. DFT studies

DFT calculations were carried out for the all the octamethyl substituted zinc phthalocyanines axially ligated by pyridine, 3-picoline, 3,4-lutidine and 3,5-lutidine derivatives (**4–7**). Fully optimized molecules of **4–7** exhibit conformations similar to that in the crystal structures. In general, the DFT optimized parameters are in good agreement with those observed in the crystal structures. Selected DFT parameters for the investigated zinc phthalocyanine derivatives are collected together with their X-ray values in Tables 2–5, whereas the whole detailed geometrical parameters are listed in Tables S1–S4 (in the SI). It should be noted that the X-ray experimental results refer to the solid phase and the DFT calculated results refer to the conformation of the molecules in the gas phase. Thus, as seen in Tables 2–5, some differences between these values can be understood. The calculated four equatorial Zn–N bond lengths are slightly longer (~0.02 – 0.03 Å), whereas the axial Zn–N bonds in these zinc phthalocyanine derivatives are longer by ~ 0.05 Å than that in the crystal structures. The deviation of the Zn(II) ion from the N_4 -isoindole plane in all Zn(Me)₈Pc-L molecules in the gas phase, as obtained by the DFT calculations, is slightly greater than that found in the crystal geometries (Table 2). However, a tendency to reduce the Zn deviation from the ring plane going from the pyridine complex (0.412 Å) to 3-picoline (0.440 Å) can be noticed. The intermediate value for the Zn deviation from the N_4 -plane was found in the Zn(Me)₈Pc-L molecules with 3,4- and 3,5-lutidine as axial ligands (0.428 and 0.425 Å).

The calculations expose two equivalent global minima and two equivalent local minima on the potential energy surface (PES). The values of the rotational barriers were derived from the variation of the total energy as a function of the rotation angle (the N2–N9–C45 torsion angle) and the results are illustrated in Fig. 6. The rotational barriers of the axial ligands (py, 3-pic, 3,4-lut and 3,5-lut) were calculated by DFT using the same basis set as for the optimization.

As can be seen from Fig. 6, during the rotation of the axial ligand around the Zn–N9 bond from 0 to 180°, two pairs of minimum of energy global (at 0 and 90°) and local (at 45 and 135°) are observed; thus the total energy of the molecule is equal for the four symmetrically equivalent conformations (the same value for the rotation from 0 to 180° as for 180 to 360°). The conformation of the Zn(Me)₈Pc-L molecules with the global energy minimum is at the rotation angle of the axial ligand when its plane coincides with the Zn–N_{iso} bond, while the local energy minima appears when the plane of the axial ligands coincides with the axis of the virtual Zn–N_{aza} bond. During rotation of the axial ligand around the Zn–N9 bond from 0 to 180°, two pairs of different rotational barriers are observed. The first energy barrier at the rotation angle of 22.5° (and equivalent at 112.5°) equals ~4.5 kJ/mol in the complexes with pyridine (**4**) and 3-picoline (**5**) and ~4.8 kJ/mol in the complexes with 3,4-lutidine (**6**) and 3,5-lutidine (**7**), whereas the second energy barrier at the rotation angle of 67.5° (and equivalent at 157.5°) is comparable with the *kT* energy (~2.5 kJ/mol). This conformational relationship is understandable by looking at the maps of the electrostatic potential as well as the interactions between H atoms in the *ortho* position to the nitrogen atom of the ligand with a slight positive EP and the macrocycle (Me)₈Pc ring with a variable EP (See Fig. 1).

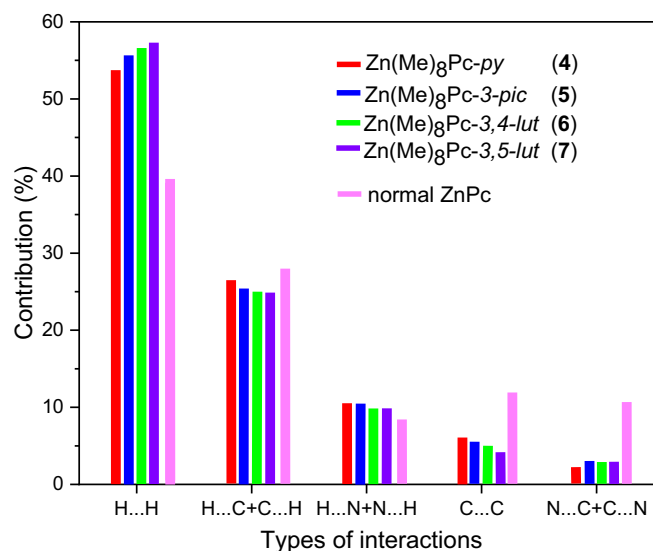


Fig. 5. Percentage contributions of the intermolecular interactions in crystals **4–7** and for comparison in the crystal of the normal ZnPc.

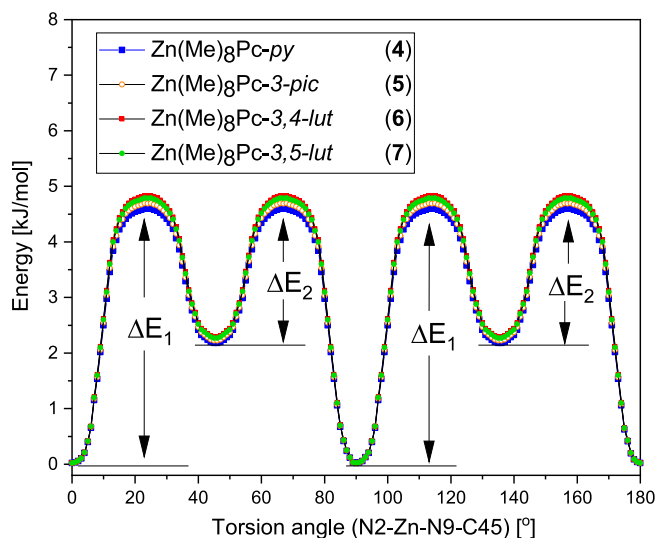


Fig. 6. Rotational barriers during rotation of the axial ligand (py, 3-pic, 3,4-lut and 3,5-lut) around the axial Zn–N9 bond (change of the torsion angle N2–Zn–N9–C45 from 0 to 180°).

3.6. UV–Vis spectroscopic characterization

To further characterize the octamethyl substituted zinc phthalocyanine derivatives **4–7**, the electronic absorption spectra were recorded. The spectra were recorded in pyridine and in toluene solutions (Fig. 7). The spectra of the investigated $\text{Zn}(\text{Me})_8\text{Pc-L}$ derivatives (**4–7**) in both solvents are very similar and show two bands (Q and B) characteristic for the phthalocyaninate(2-) macrocycle [37]. The Q and B bands are observed at ~ 680 and ~ 350 nm in both solvents (Fig. 7). The Q band corresponds to excitation between the HOMO and LUMO levels and the B band corresponds to the HOMO–1 to LUMO level transition. In addition, vibronic splitting of the Q band with a splitting value of ~ 60 nm is observed, which has been mentioned in the literature [38]. The UV–Vis spectra of the octamethyl substituted zinc phthalocyanine $\text{Zn}(\text{Me})_8\text{Pc}$ were also recorded in pyridine and toluene solutions. The maximum absorption of the Q and B bands of $\text{Zn}(\text{Me})_8\text{Pc}$ are slightly hypsochromically shifted (blue shifted), by about 6–8 nm for the Q band and by ~ 20 nm for the B-band (Fig. 7) in relation to **4–7**. So, the bathochromic shift of the axially ligated $\text{Zn}(\text{Me})_8\text{Pc-L}$ derivatives **4–7** in relation to $\text{Zn}(\text{Me})_8\text{Pc}$ may be associated with a change in the energy gap between the electronic levels as a result of axial ligation. Time-dependent DFT calculations confirm the differences in energy gaps between the electronic HOMO/LUMO levels of the unsubstituted $\text{Zn}(\text{Me})_8\text{Pc}$ and the axially ligated $\text{Zn}(\text{Me})_8\text{Pc-L}$ derivatives **4–7** (see Fig. 9 and S12, S13 and S14 in the SI).

The aggregation behaviour of the investigated complexes was examined by varying their concentration in different solvents within the limits of the Beer–Lambert's law. Usually, the aggregation of phthalocyanines occurs in any system through a coplanar association that makes the conversion of a monomer to higher order complexes, leading to insolubility in many organic solvents. This behaviour depends on the nature of the substitution, metal ions, concentration, solvent polarity and temperature of the studied system [39]. In this study, the aggregation behaviour of the zinc(II) phthalocyanine complexes peripherally octa-substituted by methyl groups and with axially ligated *N*-donor ligands was examined in pyridine and toluene solvents at different concentrations. These metallophthalocyanines have minimum aggregation in both solvents, as illustrated in Figs. S10 and S11 (SI). With the

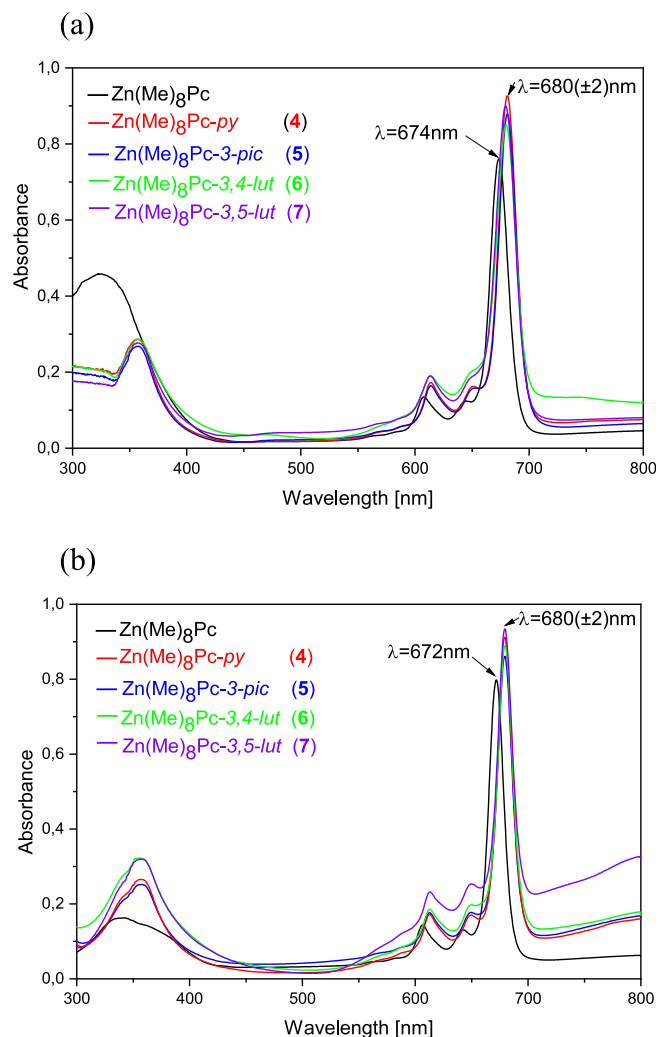


Fig. 7. UV–Vis spectra of $\text{Zn}(\text{Me})_8\text{Pc-L}$ derivatives in pyridine (a) and toluene (b) solutions.

increase in the *Pc* concentration, the intensity of absorption of the Q-band increased linearly, with no new bands and wavelengths shifts observed, which clearly indicate that there were no aggregated species [40]. This behaviour results from the effect of peripheral substitution and the axial ligation of a large ligand, leading to the deformation of the *Pc*-macrocycle from planarity, limiting the π - π interaction and preventing association.

Besides, the UV–Vis spectroscopic characterization of the investigated $\text{Zn}(\text{Me})_8\text{Pc-L}$ derivatives (**4–7**) in different solutions, diffuse reflectance spectroscopic (DSR) characterization on the solid $\text{Zn}(\text{Me})_8\text{Pc-L}$ derivatives (**4–7**) was performed. Due to the high diffuse reflectance of the **4–7** derivatives and to minimize the effects of regular reflection and particle size, the samples were diluted with non- or weak absorbing colorless standard of Al_2O_3 . The concentration of the studied $\text{Zn}(\text{Me})_8\text{Pc-L}$ derivatives (**4–7**) in the used Al_2O_3 diluent was 5% by weight. As shown in Fig. 8, the DSR spectra of $\text{Zn}(\text{Me})_8\text{Pc-L}$ derivatives (**4–7**) exhibit similar bands of similar intensities. The λ_{max} positions of the Q and B bands of the $\text{Zn}(\text{Me})_8\text{Pc-L}$ derivatives (**4–7**) are observed at 680 and 355 nm, which are bathochromically shifted in relation to the $\text{Zn}(\text{Me})_8\text{Pc}$ complex (Fig. 8). Quite a similar correlation was also found in the UV–Vis spectra in solution. However, due to the interactions between the molecules in the solid state, the DSR bands are significantly much wider in relation to the UV–Vis bands of the complexes in solution.

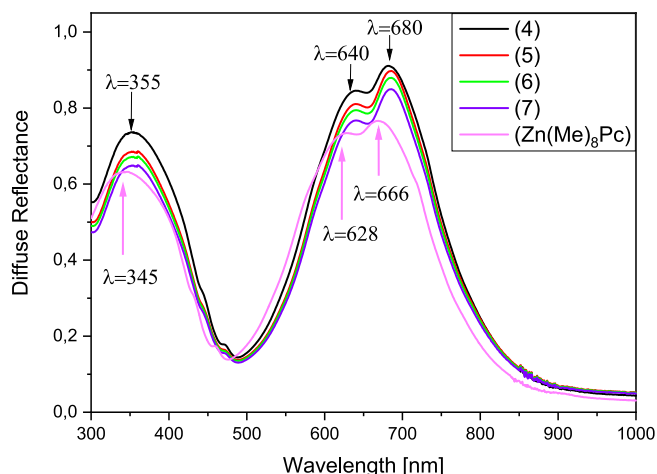


Fig. 8. UV-Vis diffuse reflectance spectra of Zn(Me)₈Pc-*L* derivatives (**4–7**) and Zn(Me)₈Pc diluted with Al₂O₃ (5%).

The broadening of the absorption bands in the solid thin films is a common feature of metallophthalocyanines, which has been widely discussed in the literature [41].

To further explore the optical properties of the Zn(Me)₈Pc-*L* complexes, time-dependent TD DFT calculations were performed. The optical absorption spectra were calculated for the all Zn(Me)₈Pc-*L* derivatives (**4–7**) as well as for Zn(Me)₈Pc and normal ZnPc for a comparison. The results are summarized in Table 6 and full details are listed in Table S6 (SI). Partial molecular energy diagrams, HOMO and LUMO frontier orbitals and the calculated electronic absorption spectra for Zn(Me)₈Pc-*py* (**4**) and Zn(Me)₈Pc are shown in Fig. 9. The calculated energy gap between the HOMO and LUMO levels is 2.0171 eV (614.66 nm) for the Zn(Me)₈Pc-*py* complex, whereas for the Zn(Me)₈Pc complex it is 2.0912 eV (592.89 nm) and a similar value is obtained for the normal ZnPc complex (2.0857 eV, 594.46 nm). The calculated energy gaps between the HOMO and LUMO levels for Zn(Me)₈Pc-3-pic (**5**), Zn(Me)₈Pc-3,4-lut (**6**) and Zn(Me)₈Pc-3,5-lut (**7**) are 2.0171 eV (614.66 nm), 2.0190 eV (614.09 nm) and 2.0172 eV (614.59 nm), respectively. Partial molecular energy diagrams, HOMO and LUMO frontier orbitals and the calculated electronic absorption spectra for Zn(Me)₈Pc-3-pic (**5**), Zn(Me)₈Pc-3,4-lut (**6**) and Zn(Me)₈Pc-3,5-lut (**7**) are shown in Figs. S11, S12 and S13 (SI) and they are very similar to that of the complex Zn(Me)₈Pc-*py* (**4**), whereas the partial molecular energy diagrams, HOMO and LUMO frontier orbitals and the calculated electronic absorption spectra for Zn(Me)₈Pc and the normal ZnPc dye are shown in Fig. S14 (SI).

A small bathochromic shift of the maximum absorption wavelength (λ_{max}) in the spectra of the Zn(Me)₈Pc-*L* complexes **4–7** in relation to Zn(Me)₈Pc dye was observed. The red-shift of about 22 nm in the spectra of **4–7** is related to the slightly decreasing energy gap in relation to Zn(Me)₈Pc that should be assigned to the axial ligation effect of the pyridine or its derivative molecules, as well as to the saucer-shaped distortion of the octamethyl substituted phthalocyaninate macrocycle. The red-shift of the maximum absorption wavelength in the spectra of these Zn(Me)₈Pc-*L* complexes (**4–7**) in relation to Zn(Me)₈Pc in solution was also observed (Fig. 7). The energy gap of the HOMO-LUMO level in the octamethyl substituted zinc phthalocyanine (Zn(Me)₈Pc) is only slightly red-shifted (~2 nm) in relation to that in the normal ZnPc dye (see Table 6 and Fig. S15). Thus, the methyl substitution effect of all eight peripheral positions of the phthalocyanine ring only slightly modifies the energy gap of the HOMO-LUMO levels and practically it does not affect the dye color of Zn(Me)₈Pc in relation

Table 6

TD-DFT results for the low-energy π - π states for Zn(Me)₈Pc-*py* (**4**), Zn(Me)₈Pc-3-pic (**5**), Zn(Me)₈Pc-3,4-lut (**6**), Zn(Me)₈Pc-3,5-lut (**7**) and for Zn(Me)₈Pc and ZnPc for a comparison.

(a) Zn(Me) ₈ Pc- <i>py</i> (4)			
λ , nm	E, eV	<i>f</i>	Contribution (weight, %) [†]
614.66	2.0171	0.4498	200 → 201 (94.6), 195 → 202 (3.4), 196 → 202 (2.9)
608.37	2.0380	0.4660	200 → 202 (95.5), 195 → 201 (3.4), 196 → 201 (2.8)
512.87	2.4174	0.0025	200 → 203 (99.8)
420.24	2.9503	0.0004	200 → 204 (99.9)
393.04	3.1545	0.0013	199 → 202 (87.7), 195 → 202 (7.3), 196 → 202 (2.4)
391.36	3.1680	0.0105	199 → 201 (33.4), 194 → 201 (32.9), 195 → 201 (28.6), 196 → 201 (3.9)
388.77	3.1891	0.0049	199 → 201 (50.4), 194 → 201 (45.0), 196 → 201 (2.1)
386.82	3.2052	0.0003	194 → 202 (85.3), 195 → 202 (10.9), 199 → 202 (3.2)
(b) Zn(Me) ₈ Pc-3-pic (5)			
λ , nm	E, eV	<i>f</i>	Contribution (weight, %) [†]
614.66	2.0171	0.4470	204 → 205 (94.6), 199 → 206 (3.3), 200 → 206 (3.0)
608.17	2.0386	0.4644	204 → 206 (94.4), 199 → 205 (3.3), 200 → 205 (3.0)
504.14	2.4593	0.0019	204 → 207 (99.8)
398.56	3.1108	0.0005	204 → 208 (99.7)
392.84	3.1545	0.0139	203 → 206 (86.4), 199 → 206 (8.1), 200 → 206 (2.1)
391.32	3.1683	0.0085	198 → 205 (33.4), 199 → 205 (28.9), 203 → 205 (19.9), 200 → 205 (28.6)
389.03	3.1870	0.0065	203 → 205 (56.0), 198 → 205 (29.6), 201 → 205 (10.7), 200 → 205 (2.2)
387.72	3.1978	0.0013	201 → 205 (86.6), 203 → 205 (6.9), 198 → 205 (3.1)
(c) Zn(Me) ₈ Pc-3,4-lut (6)			
λ , nm	E, eV	<i>f</i>	Contribution (weight, %) [†]
614.09	2.0190	0.4469	208 → 209 (94.5), 203 → 210 (3.1), 204 → 210 (3.3)
607.97	2.0393	0.4635	208 → 210 (94.4), 203 → 209 (3.1), 204 → 209 (3.3)
472.96	2.6214	0.0011	208 → 211 (99.8)
392.80	3.1565	0.0007	208 → 212 (98.3)
392.49	3.1589	0.0151	207 → 210 (84.9), 203 → 210 (8.3)
391.02	3.1708	0.0083	202 → 209 (50.3), 203 → 209 (28.7), 207 → 209 (17.3)
388.54	3.1910	0.0071	207 → 209 (59.0), 202 → 209 (29.7), 205 → 209 (7.4), 204 → 209 (2.2)
387.21	3.2020	0.0015	205 → 209 (89.1), 207 → 209 (5.9)
(d) Zn(Me) ₈ Pc-3,5-lut (7)			
λ , nm	E, eV	<i>f</i>	Contribution (weight, %) [†]
614.59	2.0172	0.4440	208 → 209 (94.6), 203 → 210 (3.1), 204 → 210 (3.3)
607.96	2.0393	0.4629	208 → 210 (94.4), 203 → 209 (3.1), 204 → 209 (3.3)
497.16	2.4939	0.0016	208 → 211 (99.8)
392.62	3.1579	0.0147	207 → 210 (85.8), 203 → 210 (8.5)
391.23	3.1691	0.0073	202 → 209 (51.9), 203 → 209 (28.8), 207 → 209 (12.9)
388.70	3.1897	0.0100	207 → 209 (69.4), 202 → 209 (24.9), 204 → 209 (3.4)
387.09	3.2030	0.0001	202 → 210 (87.4), 203 → 210 (7.1), 207 → 210 (4.9)
379.73	3.2651	0.0004	208 → 212 (70.2), 208 → 213 (26.1), 206 → 209 (2.9)
(e) Zn(Me) ₈ Pc			
λ , nm	E, eV	<i>f</i>	Contribution (weight, %) [†]
592.89	2.0912	0.4489	179 → 180 (92.6), 174 → 181 (4.5), 169 → 181 (2.9)
593.89	2.0912	0.4489	179 → 181 (92.6), 174 → 180 (4.5), 169 → 180 (2.9)
394.89	3.1397	0.0061	178 → 180 (87.9), 178 → 181 (4.1), 169 → 181 (3.3), 174 → 181 (2.7)
394.89	3.1397	0.0061	178 → 211 (87.9), 178 → 180 (4.1), 169 → 180 (3.3), 174 → 180 (2.7)
(f) ZnPc			
λ , nm	E, eV	<i>f</i>	Contribution (weight, %) [†]
594.46	2.0857	0.4084	147 → 148 (93.8), 145 → 149 (6.6)

(continued on next page)

Table 6 (continued)

(f) ZnPc λ , nm	E, eV	f	Contribution (weight, %) ^{a)}
594.43	2.0858	0.4085	147→149 (93.8), 145→148 (6.6)
373.77	3.3171	0.0137	146→148 (90.6), 137→148 (6.7)
373.77	3.3171	0.0137	146→149 (90.5), 137→149 (6.7)

*) HOMO (200), LUMO (201).

*) HOMO (204), LUMO (205).

*) HOMO (208), LUMO (209).

*) HOMO (208), LUMO (209).

*) HOMO (179), LUMO (180).

*) HOMO (147) and LUMO (148).

to ZnPc. The TD DFT calculated HOMO-LUMO transition for the all Zn(Me)₈Pc-L derivatives (**4–7**) as well as for the Zn(Me)₈Pc complex is shifted by ~ 70 nm in relation to that of the experimental values. A similar discrepancy between experimental and theoretical results is also found for other metallophthalocyanines [42].

Aromatic macrocycles, including metallophthalocyanines and especially zinc phthalocyanines and their derivatives due to their non-toxicity, have been extensively studied as photosensitizers in a non-invasive treatment called photodynamic therapy due to their strong absorption in the red region of the optical spectrum [43]. In PDT, a photosensitizer in its ground state (S_0) firstly absorbs energy and is excited to its short-lived first excited state (S_1), then it undergoes conversion to the first excited triplet state by intersystem crossing ($S_1 \rightarrow T_1$). The triplet state (T_1) of the photosensitizer transfers its energy to the surrounding biological tissue containing oxygen in its triplet ground state to the highly active singlet state, which will eventually kill targeted cells. Some criteria must be met for a photosensitizer to generate satisfactory results. First, the photosensitizer should have a strong absorption band in the therapeutic window (600–900 nm) and preferably it should be red-shifted because a higher wavelength stimulates deeper penetration. Moreover, the energy gap between T_1 and the ground singlet state (S_0) must be greater than or equal to 22.5 kcal/mol [44]. A partial molecular energy diagram, HOMO and LUMO

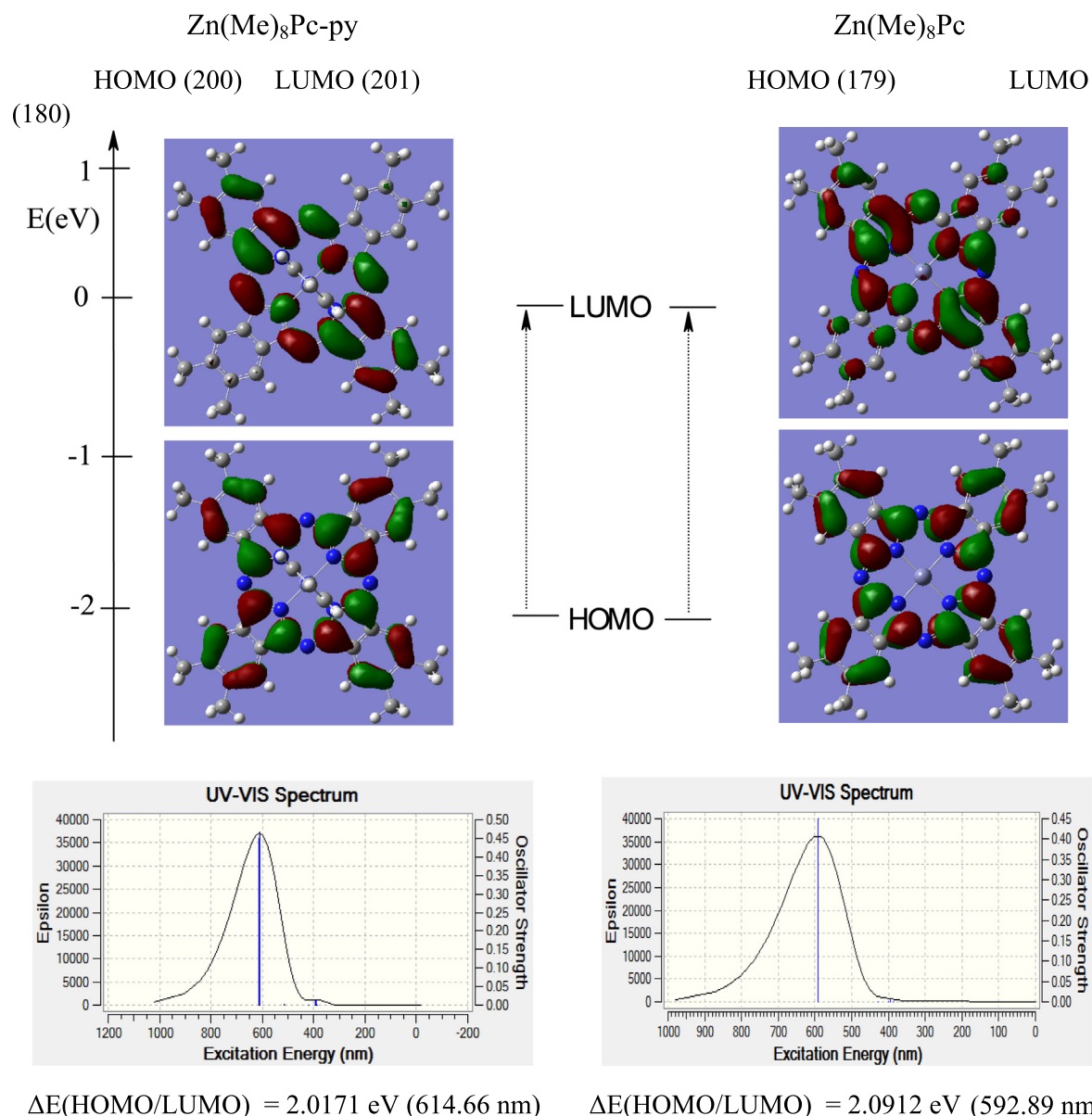


Fig. 9. Partial molecular energy diagrams, HOMO and LUMO frontier orbitals and the calculated absorption spectra for Zn(Me)₈Pc-py (**4**) and Zn(Me)₈Pc as a comparison.

frontiers orbitals and the calculated electronic absorption spectrum for $\text{Zn}(\text{Me})_8\text{Pc-py}$ (**4**) are shown in Fig. 9 and the spectra for the other complexes (**5–7**) are shown in Figs. S8–S10 (SI). The investigated complexes (**4–7**) have a strong absorption band in the therapeutic window and the HOMO–LUMO energy gap is sufficient to excite the ground state of oxygen; therefore they can be tested as potential photosensitizers for PDT.

4. Conclusion

The molecular properties of an aromatic phthalocyanine macrocycle can be significantly affected by axial binding and by methyl substituents at peripheral positions. In this work, the crystalline form of a series of methyl group octa-substituted zinc phthalocyanine complexes ligated axially by pyridine or its derivatives, $\text{Zn}(\text{Me})_8\text{Pc-L}$, were synthesized, and studied to see how the properties of the macrocycle were affected. The methyl substituents on the peripheral positions of *Pc* and the axial ligand, as a steric hindrance barrier, significantly reduce the stacking effect from $\pi\cdots\pi$ interactions relative to the unsubstituted normal zinc phthalocyanine (over 4 times), but they only improve the solubility relative to normal ZnPc by about 30%. The results reported herein are expected to provide helpful information to fields such as metal bindings in biomolecules and axially constructed materials. The central metal no longer resides within the plane after the binding of one axial ligand. The binding strength is also affected by the central metal and the macrocycle. The axial ligand donates charges to the central metal and the macrocycle when the lone pair orients along the interaction axis. This does not significantly change the singlet–triplet gap and absorption maximum. The macrocyclic M–N bondings are weakened (elongated) upon axial binding of a ligand. The bathochromic shift of the Q-band in the investigated axially ligated $\text{Zn}(\text{Me})_8\text{Pc-L}$ derivatives in relation to $\text{Zn}(\text{Me})_8\text{Pc}$ and normal ZnPc may be associated with a change in the energy gap between the electronic levels as a result of axial ligation. These metallophthalocyanines have minimum aggregation in pyridine and toluene solutions.

5. Supplementary material

Additional material contains the experimental calculated IR spectra, additional figures illustrating the inversion related dimeric structures of **4–7**, crystal packing of **4–7**, deconvolution of the 2D-fingerprint plots for individual types of interactions in the $\text{Zn}(\text{Me})_8\text{Pc-L}$ derivatives **4–7** and the optimized parameters and the TD DFT results of **4–7**. CCDC 2027869–2027872 contain the supplementary crystallographic data for **4–7**. These data can be obtained free of charge via <http://www.ccdc.cam.ac.uk/conts/retrieving.html> or from the Cambridge Crystallographic Data Centre, 12 Union Road, Cambridge CB2 1EZ, UK; fax: (+44) 1223-336-033; or e-mail: deposit@ccdc.cam.ac.uk.

CRediT authorship contribution statement

Jan Janczak: Conceptualization, Data curation, Formal analysis, Funding acquisition, Investigation, Methodology, Project administration, Resources, Software, Supervision, Validation, Visualization, Writing – original draft.

Declaration of Competing Interest

The authors declare that they have no known competing financial interests or personal relationships that could have appeared to influence the work reported in this paper.

Acknowledgment

DFT and TD DFT calculations have been carried out using resources provided by Wrocław Centre of Networking and Supercomputing (<http://www.wcss.wroc.pl>).

Appendix A. Supplementary data

Supplementary data to this article can be found online at <https://doi.org/10.1016/j.poly.2021.115024>.

References

- [1] (a) A. Thomas, *Phthalocyanine Research and Applications*, CRS Press, Boca Raton, 1990; (b) N.B. McKeown, *Phthalocyanine Materials: Synthesis, Structure and Function*, CUP, Cambridge, 1998; (c) K.M. Kadish, K.M. Smith, R. Guilard, Eds. *Handbook of Porphyrin Science*; World Scientific Publishing: Singapore, Vol. 3, pp 1–323, 2010.
- [2] (a) H. Diesbach, E. von der Weid, *Helv. Chim. Acta* 10 (1927) 886–888; (b) W. Herbst, K. Hunger, *Industrial Organic Pigments: Production, Properties, Weinheim, New York, Applications*; VCH, 1993; (c) P. Gregory, *Industrial Application of Phthalocyanines*, *J. Porphyrins Phthalocyan.* 4 (2000) 432–437; (d) P. Erk, H. Hengelsberg, in K.M. Kadish, K.M. Smith, R. Guilard (eds.), *The porphyrin Handbook*, Vol. 19: Application of Phthalocyanines. Academic Press, Amsterdam, 2003; (e) S.Z. Topal, Ü. İsci, U. Kumru, D. Atilla, A.G. Gürek, C. Hirel, M. Durmuş, J.-B. Tommasino, D. Luneau, S. Berber, F. Dumoulin, V. Ahsen, *Modulation of the electronic and spectroscopic properties of Zn(ii) phthalocyanines by their substitution pattern*, *Dalton Trans.* 43 (2014) 6897–6908.
- [3] (a) M.J. Stillman, T. Nyokong, *Absorption and Magnetic Circular Dichroism Spectral Properties of Phthalocyanines. Part 1: Complexes of Dianion, Pc(2-)*, in C.C. Leznoff, A.B.P. Lever (eds.), *Phthalocyanines: Properties and Applications*, Vol. 1, VCH Publ., New York, Weinheim, Cambridge, pp. 133–289, 1989; (b) M.J. Stillman, *Absorption and Magnetic Circular Dichroism Spectral Properties of Phthalocyanines*, in C.C. Leznoff, A.B.P. Lever (eds.), *Phthalocyanines: Properties and Applications*, Vol. 3, VCH Publ., New York, Weinheim, Cambridge, pp. 227–296, 1993; (c) K.M. Kadish, K.M. Smith, R. Guilard, Eds. *The Porphyrin Handbook*. Vol. 16: Phthalocyanines: Spectroscopic and Electrochemical Characterization. Academic Press, Amsterdam, 2003.
- [4] (a) N. Kobayashi, in *Phthalocyanines – Properties and Applications*; Leznoff, C. C., Lever, A. B. P., Eds.; VCH: New York, 1993; Vol.2, pp. 97–161; (b) N. Masilela, M. Idowu, T. Nyokong, *Photophysical, photochemical and electrochemical properties of water soluble silicon, titanium and zinc phthalocyanines*, *J. Photochem. Photobiol. A* 201 (2009) 91–97; (c) J. Chen, C. Zhu, X. Xu, P. Zhang, T. Liang, *Advances in Phthalocyanine Compounds and their Photochemical and Electrochemical Properties*, *Curr. Org. Chem.* 22 (5), (2018) 485–504; (d) G.K. Karaođlan, G. Gümrükçü, A. Koca, *The synthesis, characterization, electrochemical and spectroelectrochemical properties of a novel, cationic, water-soluble Zn phthalocyanine with extended conjugation*, *Dyes Pigments* 88(3) (2011) 247–256; (e) T. Nyokong, *Effects of substituents on the photochemical and photophysical properties of main group metal phthalocyanines*, *Coord. Chem. Rev.* 251 (2007) 1707–1722.
- [5] (a) R.A. Collins, K.A. Mohammed, *Electrical, structural and gas sensing properties of zinc phthalocyanine thin films*, *Thin Solid Films* 145(1) (1986) 133–145; (b) A. Wilson, R.A. Collins, *Electrical characteristic of planar phthalocyanine thin film gas sensors*, *Sens. Actuators* 12(4), (1987) 389–403; (c) R.A. Collins, K.A. Mohammed, *Gas sensitivity of some metal phthalocyanines*, *J. Phys. D: Appl. Phys.* 21 (1988) 154–161; (d) J. Wright, *Gas adsorption on phthalocyanines and its effects on electrical properties*, *Prog. Surf. Sci.* 31 (1989) 1–60; (e) A. Cole, R.J. McIlroy, S.C. Thorpe, M.J. Cook, J. McMurdo, A.K. Ray, *Substituted phthalocyanine gas sensors*, *Sens. Actuators B: Chem.* 13(1–3) (1993) 416–419; (f)
- [6] (a) S. Senthilarasu, S. Velumani, R. Sathyamoorthy, A. Subbarayan, J.A. Ascencio, G. Canizal, P.J. Sebastian, J.A. Chavez, R. Perez, *Characterization of zinc phthalocyanine (ZnPc) for photovoltaic applications*, *Appl. Phys. A* 77 (3–4) (2003) 383–389; (b) V.P. Singh, R.S. Singh, B. Parthasarathy, A. Aguilera, *Copper-phthalocyanine-based organic solar cells with high open-circuit voltage*, *App. Phys. Lett.* 86 (2005) 082106; (c) M.G. Walter, A.B. Rudine, C.C. Wamser, *Porphyrins and phthalocyanines in solar photovoltaic cells*, *J. Porphyr. Phthalocyanines* 14 (2010) 759–792; (d) M. Ince, J.-H. Yum, Y. Kim, S. Mathew, M. Grätzel, T. Torres, M.K. Nazeeruddin, *Molecular Engineering of Phthalocyanine Sensitizers for Dye-Sensitized Solar Cells*, *J. Phys. Chem. C* 118 (2014) 17166–17170; (e) M. Urbani, M.E. Ragoussi, M.K. Nazeeruddin, T. Torres, *Phthalocyanine for dye-sensitized solar cells*, *Coord. Chem. Rev.* 381 (2019) 1–64.
- [7] (a) G. Torre, P. Vázquez, A. Agulló-López, T. Torres, *Phthalocyanines and related compounds: organic target for nonlinear optical applications*, *J. Mater. Chem.* 8 (1998) 1671–1683; (b) H.A. Abdeldayem, D.O. Frazier, B.G. Penn, D.D. Smith, C.E. Banks, *Non-linear optothermal properties of metal-free phthalocyanine*, *Thin Solid Films* 350

- (1999) 245–248;
- (c) J.S. Shirk, R.G.S. Pong, S.R. Flom, H. Hackmann, M. Hanack, Effect of Axial Substitution on the Optical Limiting Properties of Indium Phthalocyanines, *J. Phys. Chem. A* 104 (2000) 1438–1449;
- (d) S.M. O'Flaherty, S.V. Hold, M.J. Cook, T. Torres, Y. Chen, M. Hanack, W.J. Blau, Molecular Engineering of Peripherally and Axially Modified Phthalocyanines for Optical Limiting and Nonlinear Optics, *Adv. Mater.* 15 (2003) 19–32;
- (e) B.-J. Zhou, W.-Y. Wong, D. Cui, C. Ye, Large Optical-Limiting Response in Some Solution-Processable Polyplatinaynes, *Chem. Mater.* 17 (2005) 5209–5217.
- [8] (a) P. Gregory, *High-Technology Applications of Organic Colorants*, CRC Press: Boca Raton, FL (1983);
- (b) H. Nakazumi, Organic colorants for laser disc optical storage, *J. Soc. Dye. Colour.* 104 (3) (1988) 121–125;
- (c) R. Ao, L. Kümmerl, D. Haarer, Present limits of data storage using dye molecules in solid matrices, *Adv. Mater.* 7 (5) (1995) 495–499;
- (d) H.S. Majumdar, A. Bandyopadhyay, A.J. Pal, Data-storage devices based on layer-by-layer self-assembled films of a phthalocyanine derivative, *Org. Electron.* 4 (1) (2003) 39–43;
- (e) A.A.M. Farag, Optical absorption studies of copper phthalocyanine thin films, *Opt. Laser Technol.* 39 (4) (2007) 728–732.
- [9] (a) V.J. Pansare, S. Hejazi, W.J. Faenza, R.K. Prud'homme, Review of Long-Wavelength Optical and NIR Imaging Materials: Contrast Agents, Fluorophores, and Multifunctional Nano Carriers, *Chem. Mater.* 24 (5) (2012) 812–827;
- (b) A.C.S. Lobo, A.D. Silva, V.A. Tomé, S.M.A. Pinto, E.F.F. Silva, M.J.F. Calvete, C. M.F. Gomes, M.M. Pereira, L.G. Arnaut, Phthalocyanine Labels for Near-Infrared Fluorescence Imaging of Solid Tumors, *J. Med. Chem.* 59 (10) (2016) 4688–4696.
- [10] M.M. Nicholson, in *Phthalocyanines – Properties and Applications*, C.C. Leznoff, A.B.P. Lever, Eds.: VCH, New York, Vol. 3, Chapter 2, pp 341–392, 1993.
- [11] (a) J. Blochwitz, M. Pfeiffer, T. Fritz, K. Leo, Low voltage organic light emitting diodes featuring doped phthalocyanine as hole transport material, *Appl. Phys. Lett.* 73 (1998) 729–731;
- (b) H. Kanno, T. Tsujioka, H. Takakashi, T. Usuki, Red organic light-emitting diodes using an emitting assist dopant, *Appl. Phys. Lett.* 75 (12) (1999) 1682–1684;
- (c) M. Pfeiffer, K. Leo, Z. Zhou, J.S. Huang, M. Hofmann, A. Werner, J. Blochwitz-Nimoth, Doped organic semiconductors: Physics and application in light emitting diodes, *Org. Electron.* 4 (2–3) (2003) 89–103;
- (d) Y.J. Bae, N.J. Lee, T.H. Kim, H. Cho, C. Lee, L. Fleet, A. Hirohata, Growth and characterization of thin Cu-phthalocyanine films on MgO(001) layer for organic light-emitting diodes, *Nanoscale Res. Lett.* 7 (1) (2012) 650, <https://doi.org/10.1186/1556-276X-7-650>;
- (e) J. Xu, Y. Wang, Q. Chen, Y. Lin, H. Shan, V.A.L. Roy, Z. Xu, Enhanced lifetime of organic light-emitting diodes using soluble tetraalkyl-substituted copper phthalocyanine as anode buffer layers, *J. Mater. Chem. C* 4 (2016) 7377–7382;
- (f) P.-C. Kao, S.-Y. Chu, S.-J. Liu, Z.-X. You, C.-A. Chuang, Improved Performance of Organic Light-Emitting Diodes Using a Metal-Phthalocyanine Hole-Injection Layer, *J. Electrochem. Soc.* 153 (6) (2006) H122–H126;
- (g) M. Ibrahim-Quali, F. Dumur, Recent Advances on Metal-Based Near-Infrared and Infrared Emitting OLEDs, *Molecules* 24 (7) (2019) 1412, <https://doi.org/10.3390/molecules24071412>.
- [12] (a) R. Bonnett, Photosensitizers of the porphyrin and phthalocyanine series for photodynamic therapy, *Chem Soc. Rev.* 24 (1995) 19–33;
- (b) M. Hu, N. Brasseur, S.Z. Yiildiz, J.E. van Lier, C.C. Leznoff, Hydroxyphthalocyanines as Potential Photodynamic Agents for Cancer Therapy, *J. Med. Chem.* 41 (1998) 1789–1802;
- (c) L.M. Moreira, F. Vieira dos Santos, J.P. Lyon, M. Maftoum-Costa, C. Pacheco-Soares, N. Soares da Silva, Photodynamic Therapy: Porphyrins and Phthalocyanines as Photosensitizers, *Aust. J. Chem.* 61 (2008) 741–754;
- (d) R. Bonnett, *Chemical Aspects of Photodynamic Therapy*, Gordon and Breach Science Publishers, Amsterdam, 2000;
- (e) J.D. Miller, E.D. Baron, H. Scull, A. Hsia, J.C. Berlin, T. McCormick, V. Colussi, M.E. Kenney, K.D. Cooper, N.L. Oleinick, Photodynamic therapy with the phthalocyanine photosensitizer Pc 4: The case experience with preclinical mechanistic and early clinical-translational studies, *Toxicol. App. Pharmacol.* 224 (2007) 290–299;
- (f) Y. Zhang, J.F. Lover, Recent applications of phthalocyanines and naphthalocyanines for imaging and therapy, *WIREs Nanomed. Nanobiotechnol.* 9 (2017) e1420;
- (g) V. Almeida-Marrero, E. van de Winkel, E. Anaya-Plaza, T. Torres, A. Escosura, Porphyrinoid biohybrid materials as an emerging toolbox for biomedical light management, *Chem. Soc. Rev.* 47 (2018) 7369–7400;
- (h) M.S. Pui-Chi Lo, R.K. Rodríguez-Morgade, D.K.P. Pandey, T. Ng, F. Dumoulin Torres, The unique features and promises of phthalocyanines as advanced photosensitizers for photodynamic therapy of cancer, *Chem. Soc. Rev.* 49 (2020) 1041–1056;
- (i) X. Li, B. De Zheng, X.-H. Peng, S.-Z. Li, J.-W. Ying, Y. Zhao, J.-D. Huang, J. Yoon, Phthalocyanines as medicinal photosensitizers: Developments in the last five years, *Coord. Chem. Rev.* 379 (2019) 147–160.
- [13] (a) S. Dhimi, D. Phillips, Comparison of the photophysics of an aggregating and non-aggregating aluminium phthalocyanine system incorporated into unilamellar vesicles, *J. Photochem. Photobiol., A: Chem.* 100 (1996) 77–84;
- (b) L. Howe, J.Z. Zhang, Ultrafast Studies of Excited-State Dynamics of Phthalocyanine and Zinc Phthalocyanine Tetrasulfonate in Solution, *J. Phys. Chem. A* 101 (1997) 3207–3213;
- (c) H. Kobayashi, R. Higashi, K. Ishii, K. Hatsusaka, O. Ohta, Aggregation, Complexation with Guest Molecules, and Mesomorphism of Amphiphilic Phthalocyanines Having Four- or Eight Tri(ethylene oxide) Chains, *Bull. Chem. Soc. Jpn.* 22 (1999) 1263–1271;
- (d) X.-Y. Li, A.C.H. Ng, A.K.P. Ng, Influence of Surfactants on the Aggregation Behavior of Water-Soluble Dendritic Phthalocyanines, *Macromolecules* 22 (2000) 2119–2123.
- [14] (a) F.J. Yang, X. Fang, H.Y. Yu, J.D. Wang, (4-Aminopyridine-N1) (phthalocyaninato-4N) zinc(II) tetrahydrofuran disolvate, *Acta Cryst. Sect C* 64 (2008) m375–m377;
- (b) J. Janczak, R. Kubiak, E. Bukowska, Isomorphous complexes formed by recrystallization of M(II)Pc (M(II) = Mg, Mn and Zn) in liquid 2-amino-3-picoline, *J. Mol. Struct.* 937 (2009) 25–33;
- (c) R. Kubiak, J. Janczak, M. Śledź, E. Bukowska, Comparative study of beryllium, magnesium and zinc phthalocyanine complexes with 4-picoline, *Polyhedron* 26 (2007) 4179–4186;
- (d) Q. Zeng, D. Wu, C. Wang, J. Lu, B. Ma, C. Shu, H. Ma, Y. Li, C. Bai, Bipyridine conformations control the solid-state supramolecular chemistry of zinc(II) phthalocyanine with bipyridines, *CrystEngComm* 7 (2005) 243–248;
- (e) X. Li, X. He, Y. Chen, X. Fan, Q. Zeng, Solid-state supramolecular chemistry of zinc tetraphenylporphyrin and zinc phthalocyanine with bis(pyridyl) ligands, *J. Mol. Struct.* 1002 (2011) 145–150;
- (f) T. Kobayashi, W. Ashida, N. Uyeda, E. Suito, M. Makudo, The crystal structure of the 2:3 complex of zinc phthalocyanine and n-hexylamine, *Bull. Chem. Soc. Jpn.* 44 (1971) 2095–2103;
- (g) J. Janczak, R. Kubiak, Indate (III) phthalocyanines: synthesis, spectroscopy and crystal structure of iodophthalocyaninato (2-) indate (III), *Inorg. Chim. Acta* 288 (1999) 174–180;
- (h) J. Janczak, R. Kubiak, Pyrazine control of the solid-state supramolecular chemistry of zinc phthalocyanine, *Polyhedron* 28 (2009) 23912396;
- (i) J. Janczak, R. Kubiak, Stereochemistry and properties of the M(II)-N(py) coordination bond in the low-spin dipyrindinated iron(II) and cobalt(II) phthalocyanines, *Inorg. Chim. Acta* 342 (2003) 64–76;
- (j) J. Janczak, R. Kubiak, Synthesis and characterization of dipyrindinated magnesium phthalocyaninato(2-) complex, *Polyhedron* 21 (2002) 265–274;
- (k) J. Janczak, I.M. Idemori, Synthesis, crystal structure and characterisation of aquamagnesium phthalocyanine - MgPc(H₂O). The origin of an intense near IR absorption of magnesium phthalocyanine known as X-phase, *Polyhedron* 22 (2003) 1167–1181;
- (l) V. Kinzhybalov, J. Janczak, Synthesis, structural investigation and thermal stability of aqua magnesium(II) phthalocyanine adducts with 2-methoxyethylamine, *Inorg. Chim. Acta* 360 (2007) 3314–3322;
- (m) J. Janczak, Temperature dependence on recrystallisation of the magnesium phthalocyanine (MgPc) in trimethylamine, *Polyhedron* 29 (2010) 941–949;
- (n) J. Janczak, R. Kubiak, Pyrazine control of the supramolecular chemistry of iron(II) and cobalt(II) phthalocyanines, *CrystEngComm* 12 (2010) 3599–3606;
- (o) J. Janczak, 4+1 and 4+2 coordinated complexes of magnesium phthalocyanine with dioxane, *Polyhedron* 30 (2011) 2933–2940;
- (p) B. Przybył, J. Janczak, Structural characterisation and DFT calculations of three new complexes of zinc phthalocyanine with n-alkylamines, *Dyes Pigments* 100 (2014) 247–254;
- (q) J. Janczak, Synthesis, characterisation and DFT calculations of the magnesium phthalocyanine complexes with n-butanol and n-pentanol, *Polyhedron* 70 (2014) 164–171;
- (r) B. Przybył, J. Janczak, 4+1 complexes of zinc phthalocyanine with pyridine derivative ligands, *Dyes Pigments* 118 (2015) 102–109;
- (s) B. Przybył, J. Janczak, Complexes of zinc phthalocyanine with monoaxially coordinated imidazole-derivative ligands, *Dyes Pigments* 130 (2016) 54–62.
- [15] Y.-H. Li, 1,2-Dibromo-4,5-dimethylbenzene, *Acta Cryst. E* 63 (2007) o3971.
- [16] *CrysAlis CCD and CrysAlis Red 1.171.38.43*, Rigaku Oxford Diffraction, 2015.
- [17] G.M. Sheldrick, SHELXT – Integrated space-group and crystal-structure determination, *Acta Cryst. A* 71 (2015) 3–8.
- [18] G.M. Sheldrick, Crystal structure refinement with SHELXL, *Acta Cryst. C* 71 (2015) 3–8.
- [19] K. Brandenburg, H. Putz, DIAMOND Version 3.0, Crystal Impact GbR, Bonn, Germany, (2006).
- [20] S.K. Wolff, D.J. Grimwood, J.J. MacKinnon, M.J. Turner, D. Jayatilaka, A.M. Spackman, *Crystal Explorer ver. 3.1*, University of Western Australia, Perth, Australia, 2013.
- [21] M. J. Frisch, G. W. Trucks, H. B. Schlegel, G. E. Scuseria, M. A. Robb, J. R. Cheeseman, G. Scalmani, V. Barone, B. Mennucci, G. A. Petersson, H. Nakatsuji, M. Caricato, X. Li, H. P. Hratchian, A. F. Izmaylov, J. Bloino, G. Zheng, J. L. Sonnenberg, M. Hada, M. Ehara, K. Toyota, R. Fukuda, J. Hasegawa, M. Ishida, T. Nakajima, Y. Honda, O. Kitao, H. Nakai, T. Vreven, J. A. Montgomery, Jr., J. E. Peralta, F. Ogliaro, M. Bearpark, J. J. Heyd, E. Brothers, K. N. Kudin, V. N. Staroverov, T. Keith, R. Kobayashi, J. Normand, K. Raghavachari, A. Rendell, J. C. Burant, S. S. Iyengar, J. Tomasi, M. Cossi, N. Rega, J. M. Millam, M. Klene, J. E. Knox, J. B. Cross, V. Bakken, C. Adamo, J. Jaramillo, R. Gomperts, R. E. Stratmann, O. Yazyev, A. J. Austin, R. Cammi, C. Pomelli, J. W. Ochterski, R. L. Martin, K. Morokuma, V. G. Zakrzewski, G. A. Voth, P. Salvador, J. J. Dannenberg, S. Dapprich, A. D. Daniels, O. Farkas, J. B. Foresman, J. V. Ortiz, J. Cioslowski, D. J. Fox, Gaussian, Inc., Wallingford CT, 2013. Gaussian16, Revision B.01, Gaussian, Inc., Wallingford, CT, 2016.

- [22] (a) A.D. Becke, Density-functional thermochemistry. IV. A new dynamical correlation functional and implications for exact-exchange mixing, *J. Chem. Phys.* 104 (1996) 1040–1046; (b) C. Lee, W. Yang, R.G. Parr, Development of the Colic-Salvetti correlation-energy formula into a functional of the electron density, *Phys. Rev. B* 37 (1988) 785–789; (c) B.G. Parr, W. Yang, *Density-functional Theory of Atoms and Molecules*, Oxford University Press, New York, 1989.
- [23] (a) R. Ditchfield, W.J. Hehre, J.A. Pople, Self-Consistent Molecular-Orbital Methods. IX. An Extended Gaussian-Type Basis for Molecular-Orbital Studies of Organic Molecules, *J. Chem. Phys.* 54 (1971) 724–728; (b) W.J. Hehre, R. Ditchfield, J.A. Pople, Self-Consistent Molecular Orbital Methods. XII. Further Extensions of Gaussian-Type Basis Sets for Use in Molecular Orbital Studies of Organic Molecules, *J. Chem. Phys.* 56 (1972) 2257–2261; (c) P.C. Hariharan, J.A. Pople, The influence of polarization functions on molecular orbital hydrogenation energies, *Theor. Chim. Acta* 28 (1973) 213–222; (d) P.C. Hariharan, J.A. Pople, Accuracy of AHn equilibrium geometries by single determinant molecular orbital theory, *Mol. Phys.* 27 (1974) 209–214.
- [24] (a) R. Bauernschmitt, R. Ahlrichs, Treatment of electronic excitations within the adiabatic approximation of time dependent density functional theory, *Chem. Phys. Lett.* 256 (1996) 454–464; (b) A. Dreuw, M. Head-Gordon, Single-Reference ab Initio Methods for the Calculation of Excited States of Large Molecules, *Chem. Rev.* 105 (2005) 4009–4037.
- [25] (a) E. Klingsberg, The 1,2-Dithiolium Cation; X1. Isomeric Benzodithiolium Cyanine Dyes, *Synthesis* 1 (1972) 29–30; (b) E. I. Kovshev, L. I. Solov'eva, S. A. Mikhaleenko, E. A. Luk'yanets, *Zh. Vsesoyuzn. Khim. o-va*, 1976, No. 4, 465 [Mendelev Chem. J., 1976, No. 4 (Engl. Transl.)]; (c) A.V. Ivanov, K.V. Kabanova, M.O. Breusova, I.V. Zhukov, L.G. Tomilova, N.S. Zefirov, New phosphorus-containing metal phthalocyanine complexes. Synthesis and spectral and electrochemical studies. *Russ. Chem. Bull., Int. Ed.*, 57(8) (2008) 1665–1670.
- [26] R. Kubiak, J. Janczak, A simple, novel method for the preparation of metallophthalocyanines, *J. Alloys Comp.* 200 (1993) L7–L8.
- [27] (a) P. Politzer, P.R. Laurence, K. Jayasuriya, *Molecular Electrostatic Potentials: An Effective Tool for the Elucidation of Biochemical Phenomena*, *Environ. Health Perspect.* 61 (1985) 191–202; (b) P. Politzer, D.G. Truhlar (Eds.), *Chemical Applications of Atomic and Molecular Electrostatic Potentials*, Plenum, New York, 1981; (c) J.S. Murray, P. Politzer, The electrostatic potential: an overview, *WIREs Comput. Mol. Sci.* 1 (2011) 153–163.
- [28] (a) P. Sjöberg, P. Politzer, Use of the Electrostatic Potential at the Molecular Surface To Interpret and Predict Nucleophilic Processes, *J. Phys. Chem.* 94 (1990) 3959–3961; (b) P. Politzer, J.S. Murray, In *Comput. in: Med. Chem. Drug Discovery*, Marcel Dekker Inc., New York, 2004, pp. 213–234; (c) C.A. Hunter, Quantifying Intermolecular Interactions: Guidelines for the Molecular Recognition Toolbox, *Angew. Chem., Int. Ed.* 43 (2004) 5310–5324; (d) S.A. Grimm, M. Reiher, The electrostatic potential as a descriptor for the protonation propensity in automated exploration of reaction mechanisms, *Faraday Discuss.* 220 (2019) 443–463.
- [29] (a) D.D. Perrin, *Dissociation Constants of Organic Bases in Aqueous Solution*, Butterworths, London, 1965; Supplement, 1972; (b) A. Wawrzycchów, L. Chmurzyński, A comparison of acid–base properties of substituted pyridines and their N-oxides in propylene carbonate. *J. Chem. Thermodynamics* 30 (1998) 713–722; (c) E.L. Kapinos, H. Sigel, Acid-base and metal ion binding properties of pyridine-type ligands in aqueous solution. Effect of ortho substituents and interrelation between complex stability and ligand basicity. *Inorg. Chim. Acta* 337 (2002) 131–142.
- [30] F.H. Allen, *Acta Cryst. B* 58 (2002) 380–388.
- [31] M.A. Spackman, D. Jayatilaka, Hirshfeld surface analysis, *CrystEngComm* 11 (2009) 19–32.
- [32] J.J. McKinnon, M.A. Spackman, A.S. Mitchell, Novel tools for visualizing and exploring intermolecular interactions in molecular crystals, *Acta Crystallogr., Sect. B: Struct. Sci* 60 (2004) 627–668.
- [33] J.J. McKinnon, D. Jayatilaka, M.A. Spackman, Towards quantitative analysis of intermolecular interactions with Hirshfeld surfaces, *Chem. Commun* 37 (2007) 3814–3816.
- [34] J. Janczak, Coordination properties of diethylenetriamine in relation to zinc phthalocyanine, *Polyhedron* 178 (2020) 114313.
- [35] A. Bondi, van der Waals Volumes and Radii, *J. Phys. Chem.* 68 (1964) 441–447.
- [36] J.J. McKinnon, A.S. Mitchell, M.A. Spackman, Visualising intermolecular interactions in crystals: naphthalene vs. terephthalic acid. *Chem. Commun.* (1998) 2071–2072.
- [37] L. Edwards, M. Gouterman, X.V. Porphyrins, Vapor absorption spectra and stability: Phthalocyanines, *J. Mol. Spectrosc.* 33 (1970) 292–310.
- [38] (a) T. Nykong, Z. Gasyna, M.J. Stillman, Analysis of the absorption and magnetic circular dichroism spectra of zinc phthalocyanine and the pi-cation-radical species [ZnPc(1-)]⁺, *Inorg. Chem.* 22 (1987) 1087–1095; (b) T. Reinot, J.M. Hayes, G.J. Smal, C. Zerner, Q-band splitting and relaxation of aluminum phthalocyanine tetrasulfonate, *Chem. Phys. Lett.* 299 (1999) 410–416; (c) K. Liu, Y. Wang, J. Yao, Y. Luo, Origin of the Q-band splitting in the absorption spectra of aluminum phthalocyanine chloride, *Chem. Phys. Lett.* 438 (2007) 36–40.
- [39] (a) J.A. Duro, T. Torres, Synthesis and Aggregation Properties in Solution of a New Octasubstituted Copper Phthalocyanine: {2,3,9,10,16,17,23,24-Octakis-[(diocetylaminocarbonyl)methoxy]-phthalocyaninato}-copper(II), *Eur. J. Inorg. Chem.* 126 (1993) 269–271; (b) C.A. Kernag, D.V. McGrath, Non-aggregating octasubstituted dendritic phthalocyanines, *Chem. Commun.* 34 (2003) 1048–1049; (c) C.A. Kernag, D.V. McGrath, Solution and Thin-Film Aggregation Studies of Octasubstituted Dendritic Phthalocyanines, *Isr. J. Chem.* 49 (2009) 9–21; (d) T. Wang, X. Fu Zhang, X. Lu, Metal-free phthalocyanine aggregation and binding with amines: Specific and general solvent effects on absorption and fluorescence properties, *J. Mol. Struct.* 1084 (2015) 319–325; (e) N.R.S. Gabo, T.J. Brocksom, K.T. de Oliveira, Soluble and non-aggregated phthalocyanines: synthesis, mechanistic aspects and their main building blocks, *Curr. Org. Synth.* 14 (2017) 1132–1155; (f) T.F.M. de Souza, F.C.T. Antonio, M. Zanotto, P.H. de Mello, A.O. Ribeiro, Photophysical and Photochemical Properties and Aggregation Behavior of Phthalocyanine and Naphthalocyanine Derivatives, *J. Braz. Chem. Soc.* 29 (2018) 1199–1209.
- [40] (a) C. Jing, R. Wang, H. Ou, A. Li, Y. An, S. Guo, L. Shi, Axial modification inhibited H-aggregation of phthalocyanines in polymeric micelles for enhanced PDT efficacy, *Chem. Commun.* 54 (2018) 3985–3988; (b) Z. Biyiklioglu, H. Alp, Synthesis, characterization, electropolymerization and aggregation properties of axially diethyl-dimethylaminophenoxypropanoxy substituted silicon phthalocyanines and their water soluble derivatives, *Dyes Pigment.* 132 (2016) 213–222; (c) V.F. Pais, E.F.A. Carvalho, J.P.C. Tomé, Supramolecular control of phthalocyanine dye aggregation, *J. Supramol. Chem.* 26 (2014) 642–647.
- [41] (a) A. Endo, S. Matsumoto, J. Mizuguchi, Interpretation of the Near-Infrared Absorption of Magnesium Phthalocyanine Complexes in Terms of Exciton Coupling Effects, *J. Phys. Chem. A* 103 (1999) 8193–8199; (b) J. Janczak, Y.M. Idemori, Synthesis, crystal structure and characterisation of aquamagnesium phthalocyanine - MgPc(H₂O). The origin of an intense near IR absorption of magnesium phthalocyanine known as X-phase, *Polyhedron* 22 (2003) 1167–1181; (c) J. Spadavecchia, G. Ciccarella, R. Rella, S. Capone, P. Siciliano, Metallophthalocyanines thin films in array configuration for electronic optical nose applications, *Sens. Actuators B Chem.* 96 (2003) 489–549; (d) R.J.C. Brown, A.R. Kucernak, N.J. Long, C. Mongay-Batalla, Spectroscopic and electrochemical studies on platinum and palladium phthalocyanines, *New J. Chem.* 28 (2004) 676–680; (e) Y. Açıkkbaş, M. Eyyapan, T. Ceyhan, R. Çapan, Ö. Bekaroğlu, Characterisation of Langmuir-Blodgett films of new multinuclear copper and zinc phthalocyanines and their sensing properties to volatile organic vapours, *Sens. Actuators B Chem.* 123 (2007) 1017–1024; (f) B.W. Caplins, T.K. Mullenbach, R.J. Holmes, D.A. Blank, Femtosecond to nanosecond excited state dynamics of vapor deposited copper phthalocyanine thin films, *Phys. Chem. Chem. Phys.* 18 (2016) 11454–11459; (g) K.J. Hamam, M.I. Alomari, A study of the optical band gap of zinc phthalocyanine nanoparticles using UV-Vis spectroscopy and DFT function, *Appl. Nanosci.* 7 (2017) 261–268.
- [42] (a) Y. Yang, Effects Induced by Axial Ligands Binding to Tetrapyrrole-Based Aromatic Metallomacrocycles, *J. Phys. Chem. A* 115 (2011) 9043–9054; (b) J. Janczak, Solvothermal modification of magnesium phthalocyanine, *Inorg. Chim. Acta* 478 (2018) 88–103; (c) J. Janczak, Water-Involved Hydrogen Bonds in Dimeric Supramolecular Structures of Magnesium and Zinc Phthalocyaninato Complexes, *ACS Omega* 4 (2019) 3673–3683.
- [43] (a) E. Ben-Hur, W.-S. Chan, Phthalocyanines in photobiology and their medical applications. In *The Porphyrin Handbook*; K.M. Kadish, K.M. Smith, R. Guilard, Eds.; Academic Press: Boston, 2003; vol. 19, pp 1–35; (b) W. Liu, T.J. Jensen, F. R. Fronczek, R.P. Hammer, K.M. Smith, A.G.H. Vicente, Synthesis and Cellular Studies of Nonaggregated Water-Soluble Phthalocyanines, *J. Med. Chem.* 48 (2005) 1033–1041; (c) U. Drechsler, M. Pfaff, M. Hanack, Synthesis of novel functionalised zinc phthalocyanines applicable in photodynamic therapy. *Eur. J. Chem.* (1999) 3441–3453; (d) I. Rosenthal, Phthalocyanines as photodynamic sensitizers. *Photochem. Photobiol.* 53 (1991) 859–870; (e) S. Makhseed, M. Machacek, W. Alfadly, A. Tuhl, M. Vinodh, T. Simunek, V. Novakova, P. Kubat, E. Rudolf, P. Zimcik, Water-soluble non-aggregating zinc phthalocyanine and in vitro studies for photodynamic therapy, *Chem. Commun.* 49 (2013) 11149–11151; (f) S. Moeno, R.W. Krause, E.A. Ermilov, W. Kuzniak, M. Höpfner, Synthesis and characterization of novel zinc phthalocyanines as potential photosensitizers for photodynamic therapy of cancers, *Photochem. Photobiol. Sci.* 13 (2014) 963–970.
- [44] (a) I. Lanzo, N. Russo, E. Sicilia, First-Principle Time-Dependent Study of Magnesium-Containing Porphyrin-Like Compounds Potentially Useful for Their Application in Photodynamic Therapy, *J. Phys. Chem. B* 112 (2008) 4123–4130; (b) A.D. Quartarolo, S.G. Chiodo, N. Russo, A Theoretical Study of Brominated Porphycenes: Electronic Spectra and Intersystem Spin–Orbit Coupling, *J. Chem. Theory Comput.* 6 (2010) 3176–3189.